ONCOGENIC PROPERTIES AND TARGETING OF *NTRK1* IN BREAST CANCER

by
Kelly Kyker-Snowman

A dissertation submitted to Johns Hopkins University in conformity with the requirements for the degree of Doctor of Philosophy

Baltimore, Maryland
March 2018

Abstract

Triple negative breast cancers (TNBC) comprise a highly aggressive cancer subtype with high mortality rates, high frequency of metastatic disease and a lack of targeted therapies. A fraction of these cancers also demonstrate amplification of the *NTRK1* gene. The protein product of the *NTRK1* gene, TrkA, is a receptor tyrosine kinase (RTK) that recognizes neuronal growth factor (NGF) leading to downstream signaling through MAPK and other pathways that promote survival and proliferation. Pan-Trk inhibitors have been developed against rare cancers with *NTRK* translocations that result in constitutive Trk kinase activity. Expansion of these inhibitors' application to amplifications, particularly in TNBC, offers the potential for targeted therapies. Here, we engineered non-tumorigenic immortalized human mammary epithelial cell lines and human breast cancer cell lines to overexpress TrkA. Overexpressing clones demonstrated cancerous and pro-metastatic phenotypes, which were reversed upon exposure to the Trk inhibitor larotrectinib. *In vitro*, the MCF10A and hTERT-IMEC engineered cell lines showed growth factor independence, increased downstream proliferative and pro-survival signaling, alterations in three-dimensional culture, and migratory phenotypes in increased wound healing and microchannel migration. *In vivo,* TrkA-overexpressing MCF7 cells

showed increased tumor growth and acquired the capacity to establish disseminated disease. Our results demonstrate the potential clinical utility of larotrectinib for targeting *NTRK1* amplified breast cancers and inhibiting metastasis.

Thesis Advisor: Ben Ho Park, M.D., Ph.D.

Thesis Readers: Ben Ho Park, M.D., Ph.D.

Ie-Ming Shih, M.D., Ph.D.

Acknowledgements

This dissertation would not have been completed without the critical support of many, many people – to each of you, and many more, I owe my sincerest thanks.

To Ben, who has built a lab that values relationships and play as critical to research and innovation, and who takes the time to teach as well as lead. Ben's encouragement of mentoring other labmates, and interrogative teaching style, has developed in me an independent intellect and a drive to discover more.

To my lab colleagues, and their willingness to share knowledge and experimental techniques, as well as snacks.

To my dance family, who balance out all the science and lighten my heart, and have given me the freedom to get comfortable with creativity and a gateway to engage with the incredible talent of Baltimore's youth.

To my mom, who was the first to teach me that women lead, whether in rock climbing and paddling or in science. I hope that I have done her proud, and it is her memory that drives me to this work. Her embodiment of joy and insistence on the pleasure of working hard seeded in me early and has provided the foundation for getting through graduate school.

To my dad. My dad has been my best editor and most talented model for writing well since my early forays into published literature ("Zippy's Big Adventure", a harrowing tale of pet bunny bravery). He listens avidly to all of the detailed steps of investigating a scientific system, and is always available for unparalleled pep talks when it gets frustrating. He is my highest cheerleader and my most important support. I don't know anyone else who would have read and reread this dissertation for grammar and formatting, and I am grateful for that and so much more.

To my sister, Emily. Em challenges me intellectually and keeps me grounded in the roots of what it means to have the woods of Massachusetts as home. She reminds me that if we can survive winter camping and build a house from the ground up, then a research career is no insurmountable challenge. Her curiosity about my research systems and her brilliance about hers encourages me to read more broadly and learn more deeply in order to teach more thoroughly. She inspires me often.

To my family, who have believed in my brilliance without ever faltering since before I could talk. They nourish me daily with their energy, their love, and their joy.

Table of Contents

Preface

Title……..……...……..i

Abstract……...……..……ii

Acknowledgements…….……iv

Table of Contents..……..…….……vi

List of Tables……..……..……...vii

List of Figures…….…...viii

Chapters

Chapter 1: Introduction……..……..1

Chapter 2: Materials and Methods……..……...7

Chapter 3: Results…….....17

Chapter 4: Discussion……...……68

References……72

Curriculum Vitae……..……..81

List of Tables

Table 1: Cell lines used in this study……..……..28

Table 2: Primers used in this study…….....29

Table 3: Frequency of *NTRK1* amplification in breast cancers via cBioPortal…..30

Table 4: Genes upregulated in TrkA-overexpressors by microarray.....31

Table 5: Genes downregulated in TrkA-overexpressors by microarray.....32

List of Figures

Figure 1: Experimental design…….…….33

Figure 2: TrkA modifications in breast cancer, TCGA…….…….34

Figure 3: Kaplan-Meier curve for TCGA data, breast cancer, *NTRK1*…….....35

Figure 4: Growth factor independence crystal violet in MCF10A cell lines……..36

Figure 5: Growth factor independence in hTERT-IMEC cell lines…….……37

Figure 6: Proliferation in MCF10A cell lines with NGF…….....38

Figure 7: Proliferation in MCF10A cell lines with 0.2ng/mL EGF, NGF…….....39

Figure 8: Proliferation in MCF10A cell lines with larotrectinib, NGF…….....40

Figure 9: Proliferation in hTERT-IMEC cell lines with NGF……..…..……41

Figure 10: Proliferation in hTERT-IMEC cell lines with larotrectinib, NGF…..…42

Figure 11: Immunohistochemistry for TrkA of cell lines…….…43

Figure 12: Immunoblotting of MCF10A cell lines with NGF……...44

Figure 13: Immunoblotting of MCF10A cell lines with 0.2ng/mL EGF, NGF…...45

Figure 14: Immunoblotting of MCF10A cell lines with larotrectinib, NGF..…….46

Figure 15: Immunoblotting of hTERT-IMEC cell lines with NGF…….....47

Figure 16: Immunoblotting of hTERT-IMEC cell lines with larotrectinib, NGF...48

Figure 17: MCF10A-derived clone morphology in 3D culture……..……..49

Figure 18: hTERT-IMEC-derived clone morphology in 3D culture…….....50

Figure 19: MCF10A-derived clone anchorage-independent growth..…….....51

Figure 20: hTERT-IMEC-derived clone anchorage-independent growth..……52

Figure 21: Wound healing assay for MCF10A-derived clones……53

Figure 22: Wound healing assay for hTERT-IMEC-derived clones..……..54

Figure 23: Representative wound healing assay images MCF10A clones…….55

Figure 24: Microchannel migration assay speed results……...56

Figure 25: Microchannel migration assay persistence results……..……57

Figure 26: Microchannel migration assay velocity results……...…….58

Figure 27: Proliferation advantage recapitulated in *CD74-NTRK1* model…….....59

Figure 28: Immunohistochemistry of *CD74-NTRK1* fusion model…….60

Figure 29: Immunoblotting of *CD74-NTRK1* fusion model…….……61

Figure 30: *CD74-NTRK1* fusion morphogenesis in 3D culture……....62

Figure 31: Wound healing advantage recapitulated in *CD74-NTRK1* model…..63

Figure 32: TrkA overexpression confers insulin independence in MCF10A…….64

Figure 33: Xenograft assay results, solid tumors...……..……..65

Figure 34: Representative images of lungs, empty vector MCF7, tail vein...…….66

Figure 35: Representative images of lungs, TrkA-overexpressing MCF7……..67

1 Introduction

Breast cancer background

Breast cancer represents one of the leading causes of cancer mortality among women globally, with 1.2 million cases worldwide and 540,000 new diagnoses annually, causing 500,000 deaths (1). Triple negative breast cancers (TNBC), which do not express ER (estrogen receptor-alpha), PR (progesterone receptor), or targetable levels of HER2 (human epidermal growth factor 2) represent a particular challenge as a highly aggressive form of breast cancer with high rates of recurrence, metastasis and mortality (2). TNBC generally have poor outcomes and an aggressive disease course with options for therapy limited to surgical intervention, radiation and cytotoxic chemotherapies. Unlike breast cancers expressing ER/PR and/or overexpressing HER2, these cancers are

generally not candidates for treatment with targeted therapies such as trastuzumab and hormonal therapies (2-4). In spite of robust response to first line surgical and chemotherapeutic treatment, TNBC frequently recur and metastasize. After the establishment of treatment-resistant tumor populations, patients are left with few options, and no targeted therapies are currently available. TNBC is particularly common in patients with germline mutations in the *BRCA1* gene, and TNBC also have a high rate of somatic *TP53* mutations (5, 6).

Cancer formation is generally understood to result from the accumulation of somatic mutations which in combination produce a proliferative, replicatively immortal, cell death resistant tumor cell population which can evade growth suppression and the immune system, promote angiogenesis, and invade and metastasize. The genomic instability underlying the progression to these characteristics also results in a multitude of mutations in many cancer cells. Tumors accumulate mutations which independently promote tumorigenesis, termed driver mutations, and those which do not, termed passenger mutations (7). Driver mutations are further divided into oncogenes, which provide a growth advantage by their amplification or overexpression, and tumor suppressors, which promote tumorigenesis by their absence through suppression or loss of function mutation. Although driver mutations represent the most

promising targets for the development of targeted therapies, passenger mutations may equally find research utility as targets or detectable markers of tumor burden (7). TrkA amplification, the subject of this research, is a putative driver mutation in cancer (1).

TrkA background and function

TrkA translocations

TrkA was first identified in the cancer context as the unknown protein kinase component of an oncogenic fusion protein in two colon cancer patients in 1982 (1). This translocation, producing transformation in NIH-3T3 cells, was later identified by cloning and sequencing as a fusion between tropomyosin and TrkA. Oncogenic gene fusions incorporating the 3' tyrosine kinase region of TrkA remain the best characterized TrkA alterations in cancer, arising at a low to moderate level among a range of cancer types and resulting in ligand-independent, constitutively activated proliferation and survival pathways. Oncogenic rearrangements of *NTRK1* have been identified by targeted next generation sequencing (NGS) in a number of cancers, resulting in constitutive activation and downstream signaling (1, 8). The incidence of such translocations motivated the development of pan-Trk inhibitors, such as larotrectinib. Pan-Trk

inhibitors have shown promising early results in clinical trials (9, 10) as targeted therapies.

TrkA Amplifications

TrkA amplifications or copy number increase arise in a variety of cancers, reported at rates up to 22% in breast cancers according to cBioPortal (Figure 2, Table 3). Although a relatively small percentage, this represents tens of thousands of newly diagnosed patients each year in the United States alone. In TCGA data from 2015, TrkA alterations comprised primarily of amplifications correlated to a 40 month survival disadvantage (Figure 3). In addition, research has demonstrated that genetic alterations in a small percentage of cancers can lead to dramatically improved outcomes with appropriate targeted therapies, for example, EGFR mutations in non-small cell lung cancers (11). When interrogated specifically for breast cancers lacking HER2, ER, and PR expression (TNBC), rates of TrkA amplification were as high as 22% in some studies (Table 3). The mechanism of these pan-Trk inhibitors targets the kinase function of the Trk molecules by blocking the ATP binding site, and would therefore be expected to also inhibit Trk-amplified cancers.

TrkA gene and protein structure

Tropomyosin receptor kinase A (TrkA), encoded by *NTRK1* is the membrane-bound receptor tyrosine kinase (RTK) that serves as a high affinity receptor for the neuronal growth factor (NGF) (12). *NTRK1* is located on chromosome 1q23.1 and contains 16 exons, all coding. The predominant transcript variant encodes a 2492 base pair mRNA which is translated to an 87.5 kDa membrane-bound high affinity receptor comprised of 796 amino acids. TrkA is a member of the tropomyosin kinase receptor family, which also includes TrkB and TrkC, encoded by NTRK2 and NTRK3 respectively. Trk family receptors are comprised of an extracellular domain, a single transmembrane domain, and an intracellular domain. The high level of homology within this family is reflected in the extracellular domain of each member, which contains two cysteine clusters bracketing three leucine-rich motifs, and two immunoglobin-like C2 regions. The ATP binding site, which is the target for larotrectinib, is located within the intracellular domain. These receptors exist in a dynamic equilibrium between the lower ligand affinity monomeric form and the higher affinity dimeric form. Binding of the ligand (in the case of TrkA, dimeric NGF) stabilizes the dimeric form and results in downstream kinase signaling.

TrkA mediated signaling

Following binding of the ligand and dimerization, autophosphorylation of tyrosine residues Y490 and Y785 of TrkA permits binding of adaptor molecules including Shc and PLC-g, resulting in downstream catalytic activation of the Ras/MAP Kinase and PI3K pathways, promoting proliferation and survival (13). The normal physiologic function for this pathway is in the development of neuronal tissues during organogenesis, promoting survival, differentiation and proliferation of neurons in the central and peripheral nervous systems. However, when inappropriately or constitutively activated, these signaling cascades promote growth and survival in tumors. A putative autocrine loop for this signaling pathway has been identified in breast cancer (14).

Early positive results from clinical trials

Targeted therapeutics inhibiting the *NTRK* translocations have been developed with promising results recently reported (1, 8, 15, 16), and clinical trials have shown early positive results (10). The potential to expand these targeted medications to other, difficult to treat cancers offers possibilities for more directed and effective treatment.

2 Materials and Methods

Cell Culture:

The non-tumorigenic human breast epithelial cell line MCF10A and its derivatives were cultured in DMEM/F12 (1:1) supplemented with 1% Penicillin-Streptomycin (Life Technologies, Carlsbad, CA), 0.1 ng/uL cholera toxin (Sigma-Aldrich, St Louis, MO), 10ug/mL insulin (Life Technologies), 20 ng/mL EGF (Sigma-Aldrich), 0.5 ug/mL hydrocortisone (Sigma-Aldrich) and 5% horse serum (Life Technologies). The non-tumorigenic, human TERT-immortalized human breast epithelial cell line hTERT-IMEC and its derivatives were cultured in DMEM/F12 supplemented with 1% Pen/Strep, 10% charcoal-dextran stripped

fetal bovine serum (FBS) (Life Technologies), cholera toxin, insulin, hydrocortisone and EGF, with recovery for 24 hours in MCF10A media after trypsinization for plating or passaging. The human breast cancer cell line MCF7 and its derivatives were cultured in DMEM supplemented with 1% Pen/Strep and 5% FBS. *NTRK1*-overexpressing clones and *CD74-NTRK1* fusion expression clones were continuously cultured under Geneticin (Life Technologies) selection, beginning 24 hours after transfection. MCF10A parental, hTERT-IMEC parental, and MCF7 parental were purchased from ATCC.

hTERT-IMEC-derived cell lines were prepared for growth factor-reduced assays by a 48-hour arrest in DMEM/F12 with 5% charcoal/dextran stripped FBS (C/D FBS), 1% Pen/Strep, hydrocortisone, and cholera toxin after being trypsinized, spun down and washed twice with HBSS. MCF7-derived cell lines for low growth factor experiments were prepared for plating by a 48-hour arrest in DMEM with 5% C/D FBS, 1% Pen/Strep, after being trypsinized, spun down and washed twice with HBSS. MCF10A-derived cell lines were prepared for plating for low growth factor conditions (physiologic EGF and no EGF) by trypsin and two HBSS washes and spins (17).

Parental cell lines were authenticated by short tandem repeat profiling analysis at the Johns Hopkins Genetic Resources Core Facility. A complete list of cell lines generated and used in this study can be found in Table 1.

Overexpression of *NTRK1* or *CD74-NTRK1* cDNA in human cells:

NTRK1 cDNA was purchased as pCMV6-AC-GFP-NTRK1 (RC213091, Origene, Rockville, MD) and subcloned into the pIRESneo3 vector (Clontech, Mountain View, CA) by amplification (Table 2) and addition of cut sites before digestion and ligation into pIRESneo3. Cells were transfected with pIRESneo3-NTRK1 using the Fugene 6 system (Promega, Fitchburg, WI). 24 hours after transfection, cells were trypsinized and changed to selection media containing Geneticin (Life Technologies) and allowed to grow until colonies were visually identified, at which point single cell selection was performed and multiple single clones were isolated. This procedure was repeated in each cell line with the pIRESneo3 empty vector as a control (17). *CD74-NTRK1* fusion cDNA was generously provided by Pasi A Janne (8). Transfection and selection were performed as above.

Immunoblotting:

Cells were washed twice with HBSS (Life Technologies) and plated at 500,000 cells per well in 6-well plates. After 24 hours, media was changed to specified conditions. 24 hours after media change, cells were harvested for protein lysates and immunoblotting was performed as previously described (17). Briefly, cells were washed twice with HBSS and collected in Laemlli buffer

(Invitrogen, Carlsbad, CA) with 10% beta mercaptoethanol, placed at 100C for 10 minutes and frozen. Protein was quantified with Pierce 660nM Reagent (Invitrogen) and lysates loaded accordingly into NuPage 4-12% gel (Invitrogen) and run at 200V for 35 minutes. Gels were transferred to polyvinylidine difluoride (PVDF) 45uM membranes (Invitrogen) for 1 hour at 30V. Membranes were blocked with 10% milk in TBST for 1 hour, placed in primary antibody in 5% milk at 4C overnight, washed 4x5 minutes in TBST, placed in horseradish peroxidase-conjugated secondary antibody in 5% at room temperature for 1 hour, washed 20 minutes with TBST, 2x5 minutes in TBST, 5 minutes in TBS, and finally placed in ECL reagent solution for 1 minute before exposure of X-ray film for visualization.

The primary antibodies used in this study include anti-TrkA rabbit antibody (2505; Cell Signaling Technology, Danvers, MA), anti-pTrkA rabbit antibody (9141S; Cell Signaling), anti-hSerpin E1/PAI-1 mouse antibody (MAB 1786; R&D Systems, Minneapolis, MN), anti-phospho-AKT rabbit antibody (9271; Cell Signaling), anti-AKT rabbit antibody (9272; Cell Signaling), anti-phospho-p44/p42 MAP kinase rabbit antibody (4370; Cell Signaling), anti-p44/p42 MAP kinase rabbit antibody (9102; Cell Signaling), anti-phospho-P90RSK rabbit antibody (9341; Cell Signaling), anti-P90RSK rabbit antibody (9333; Cell Signaling), anti-phospho-p70 S6 kinase rabbit antibody (9205; Cell

Signaling), anti-p70 S6 kinase rabbit antibody (9202; Cell Signaling), and anti-GAPDH rabbit antibody (5174; Cell Signaling) (17, 18).

Cell proliferation assays:

Cell counting:

Exponentially growing cells were washed twice in HBSS before plating at 30,000 cells/well in 12-well plates in triplicate. After 24 hours, media was changed to specified conditions. Cells were trypsinized and counted using a Beckman-Coulter cell counter at days 2, 4, and 6 after plating (17). Assay media, DMEM/F12 supplemented with 1% penicillin-streptomycin, 10% charcoal-dextran stripped fetal bovine serum (Life Technologies), 0.1 ng/uL cholera toxin, 0.5 ug/mL hydrocortisone, 10ug/mL insulin for MCF10A. Epidermal growth factor (EGF) added at 0.2 ng/mL. NGF, neuronal growth factor, 100ng/mL for MCF10A-derived cells, 12.5ng/mL for hTERT-IMEC derived cells.

Crystal violet:

Cells were plated at 30,000 cells/well in 24-well or 48-well plates. As appropriate, media was replaced with media containing drug at 24 hours after plating. At 1 week, cells were washed twice with HBSS before addition of a .05% crystal violet solution in 70% ethanol for 15 minutes, rinsed, allowed to dry, and

imaged (17). Images were taken from larger plates in smaller groups to avoid parallax effect.

Colony formation in semisolid media:

A solution of cells at 30,000 cells/mL media was prepared and mixed 1:1 with a 1x media, 1.2% UltraPure Agarose (Life Technologies) solution before plating on top of a layer of 0.6% agarose solution. After solidifying, media was added on top and replaced weekly over a course of 2-4 weeks before staining with .05% crystal violet in 70% ethanol and imaging. Colonies were counted in each field of view in each of four 10x images per well per replicate. Photographs were taken with a Nikon SMZ 1500 stereoscopic zoom microscope (17).

Acinar morphogenesis assay:

Acinar morphogenesis assays were performed with growth factor reduced Matrigel (BD Biosciences, San Jose, CA) as previously described (17). Briefly, a solution of 4% Matrigel in media with 30,000 cells/well was plated in 8-well chamber slides on top of a layer of 4% Matrigel in media. Media with Matrigel in appropriate conditions was added weekly over a course of 1-4 weeks and images taken at appropriate time points at 40x with a Nikon SMZ 1500 stereoscopic zoom microscope (17).

Wound healing assay:

Cells were plated at 2 million cells/well in 6-well plates and checked for confluence the following day. Scratch wounds were made in a cross pattern using a 200uL pipette tip and media changed to conditioned or drugged media. Phase contrast images were taken to the left or right of the center of the cross wound at 10x at 0 hour and 16 hour time points. Scratch size in each image was quantified using the Scratch Assay Analyzer tool in the MiToBo extension in ImageJ 2.0 with sigma = 2 and entropy filter = 25 and verified by hand. The percent of wound healing was calculated by dividing the wound area at 16 hours by the wound area at 0 hours, subtracting the resulting value from 1, and multiplying by 100 (17).

Microchannel migration assays:

A polydimethylsiloxane (PDMS) microfluidic device was produced by standard photolithography and replica molding, comprised of an array of microchannels 200um long, 10um tall, with widths of 3um, 6um, 10um, 20um, or 50um, as previously described (17). Prior to cell seeding, the PDMS device and glass coverslip were plasma cleaned, and the PDMS device was adhered to the glass surface. Collagen Type I (BD Biosciences) at 20 ug/mL in phosphate buffered saline (PBS) was absorbed for one hour at 37C, then aspirated and

washed with PBS before cell seeding. Cells were trypsinized, washed with HBSS and suspended at 50,000 cells in 50uL low growth factor media (DMEM with 2% C/D FBS, 1% Pen/Strep) in a well at one end of the device. The well at the opposite end was filled with full growth factor media with NGF. Time-lapse microscopy images were taken at 10 minute intervals for 12 hours. Cell bodies were identified by hand in each frame with the x-y position of a cell defined by the central cell body, and values for cellular velocity, displacement and distance traveled were calculated with a custom MATLAB program (17).

Immunohistochemistry:

Confluent T75 flasks were trypsinized and centrifuged to form cell pellets. Cell pellets were fixed in formalin for 24 hours before paraffin embedding, sectioning and adherence to slides. Slides were steamed in EDTA solution and incubated with anti-TrkA rabbit monoclonal antibody (2505S; Cell Signaling). Poly-HRP anti-rabbit IgG antibody was applied and then visualized with 3,3'-diaminobenzidine (Sigma). Slides were counterstained with hematoxylin (18).

Xenograft assays:

For each group, a minimum of five 8- to 10-week old female athymic nude mice (Harlan Laboratories, Indianapolis, IN) were provided with estrogen pellet supplementation prior to cell injection. For solid tumor formation studies, cell

solutions were prepared in a 20% sterile PBS, 80% growth factor-reduced Matrigel (BD Biosciences) containing 1 million cells/200uL and injected subcutaneously in either flank at 200uL. Tumor volumes were measured weekly and calculated by multiplying width, length and height for each individual tumor.

For tail vein injection assays, cell suspensions were prepared in sterile PBS at .5 million cells/200uL and injected at 200uL into the tail vein of 8- to 10-week-old female athymic nude mice. Mice were monitored for signs of disseminated tumor formation including palpable mass and discomfort, and euthanized as appropriate. Tissues and tumors were excised and fixed in 10% formalin before embedding in paraffin, sectioning, and staining with hematoxylin and eosin. Tissues were examined grossly, and 5 stained sections were examined for evidence of multicellular, proliferating disease per experimental group under a phase contrast microscope.

All animal experiments were performed in accordance with institutional and The National Institutes of Health Guide for the Care and Use of Laboratory Animals guidelines.

Statistics:

All statistical analyses were performed using GraphPad Prism 5 software (GraphPad Software). Unpaired Student's T tests, 1-way ANOVA, and 2-way ANOVA tests were used to compare experimental groups to the appropriate control. Significance levels are indicated by asterisks: P<= 0.05 (*), P<= 0.01 (**) and P<= 0.001 (***). Error bars represent +/- SEM.

3 Results

Overexpression of TrkA protein in non-tumorigenic human breast epithelial cell lines

With the goal of producing a breast cell model demonstrating the impact of TrkA overexpression, two non-tumorigenic human breast cell lines were transfected with a pIRESneo3 plasmid containing a human full length *NTRK1* cDNA, single cell isolated and confirmed to express the TrkA protein by western blot and immunohistochemistry of cell pellets (Figure 1, Figure 11). MCF10A is a spontaneously immortalized mammary cell line that grows best in media containing supraphysiologic (20ng/mL) epidermal growth factor (EGF), insulin,

and cholera toxin. hTERT-IMEC is a mammary cell line immortalized by human TERT protein expression that is similarly non-tumorigenic in immunocompromised mice and is grown in similar media factors. Neither parental cell line expresses the TrkA protein at significant levels, as confirmed by western blot and immunohistochemistry of cell pellets. For each of these two parental cell lines, four independent TrkA-overexpressing clones were isolated (referred to as MN1-4 and HIN2-5) as well as one empty vector control expressing the pIRESneo3 plasmid containing no cDNA (MEV and HIpI) (Figure 1). TrkA-overexpressing and empty vector clones were continuously maintained under Geneticin selection. The MCF10A cell line arrests under growth factor restricted conditions in media lacking EGF and replacing horse serum with charcoal/dextran stripped (C/D) fetal bovine serum (FBS). The hTERT-IMEC cell line takes several days to arrest under these conditions, and thus these cells were prepared for assays by plating in these conditions for 48 hours before plating for assays. As an additional positive control, MCF10A cells were transfected with a plasmid containing *CD74-NTRK1* translocation cDNA, and three clones isolated (CDN2-4) (Figure 28).

Non-tumorigenic breast cells show growth factor-independent growth when overexpressing TrkA

Parental MCF10A and hTERT-IMEC require supraphysiologic EGF as well as insulin in order to grow well. Growth factor independence represents a hallmark of cancer, and EGF independence is a phenotype that has been previously produced in MCF10A-derived cell lines when transformed by oncogenic mutations (19). In order to determine whether this was a characteristic imparted by TrkA overexpression, we performed several cell growth assays comparing TrkA overexpressing and fusion expressing cell lines to the parental cell lines under growth-factor limited (physiologic EGF, 0.2 ng/uL) and arrest (no EGF, no insulin) conditions.

In cell growth assays by crystal violet staining and by cell counting, the TrkA-overexpressing MCF10A and hTERT-IMEC and *CD74-NTRK1*-expressing MCF10A show proliferation under EGF-free growth limiting conditions as compared to arrest media in the parental and empty vector controls (Figures 4-10, Figure 27). This effect is replicated in the MCF10A cell lines under media conditions with physiologic EGF (0.2ng/mL), where the TrkA overexpressors outgrow the slow proliferation of the parental and empty vector controls. In repeating the growth assays in media lacking both EGF and insulin, here we demonstrated that TrkA overexpression results in both EGF independence and

insulin independence (Figure 32). In each of these conditions, the addition of the TrkA ligand neuronal growth factor (NGF) increases the growth advantage observed. Treatment with larotrectinib diminishes or reverses this growth factor independence phenotype. TrkA overexpression in human epithelial breast cells produces EGF and insulin-independent growth that can be effectively targeted with the inhibitor larotrectinib.

TrkA-overexpressing clones show amplified signaling in growth and survival pathways

Downstream of TrkA activation and phosphorylation are the pro-growth and pro-survival MAPK (via ERK-RSK1) and AKT (via AKT-P70S6K) pathways. Assaying for phosphorylated forms of these pathway proteins by western blot gives a clear picture of increased activation in the TrkA-overexpressing and translocation expressing clones (Figures 12-16, Figure 29). This is particularly amplified in the presence of NGF for the TrkA overexpressors, and diminished or abolished with the addition of larotrectinib even in the presence of NGF. Specifically, levels of phospho-TrkA, phospho-AKT, phospho-P70S6K, phospho-ERK, and phospho-P90RSK1 are elevated by TrkA-NGF in the MCF10A-derived cell lines, whereas the phospho-AKT phenotype was not observed in the hTERT-

IMEC-derived cell lines and the P90RSK1 expression was too low under growth factor reduced conditions to detect.

Increased irregularity and amplified anchorage-independent growth in three-dimensional culture

When cultured at low density in Matrigel under low growth factor conditions, the parental and empty vector expressing MCF10A and hTERT-IMEC form relatively small, regular spherical acini. By comparison, the TrkA-overexpressing and translocation expressing clones form larger and more irregular colonies that are frequently connected to each other or spiculated (Figures 17, 18, Figure 30). This effect is particularly pronounced in TrkA overexpressing clones in the presence of NGF, which resulted in many interconnected colonies for the MCF10A and formations like nodes connected by relatively long bridges for the hTERT-IMEC. These effects were blocked by the addition of larotrectinib, which restored even the clones in the presence of NGF to small, regular spheroids.

When cultured in soft agar, once again parental and empty vector expressing cells formed a few, regular spheres in each field of view. TrkA overexpressing and translocation lines formed many more and larger colonies, demonstrating not only increased growth rates but also increased anoikis

resistance and anchorage-independent growth (Figures 19, 20). These effects were increased in the TrkA-overexpressing cells in the presence of NGF and reduced or ablated in the presence of the inhibitor larotrectinib in overexpression and translocation clones.

Increased wound healing and migration

As one of the first stages of metastasis requires cells to migrate from the central tumor body to the circulation, migratory capacity may be indicative of a possible metastatic phenotype. Under growth-factor limited conditions, the parental MCF10A and hTERT-IMEC show reduced capacity for scratch-wound healing. In order to determine whether the migratory capacity of the overexpression clones was altered, we performed scratch wound healing and microchannel migration assays. When plated to a confluent monolayer and scratched to mimic a wound, followed by imaging over time, an increased migration and wound healing phenotype was observed in the TrkA-overexpressing and translocation cell lines (Figures 21, 22, Figure 31). An interesting change in morphology while migrating was observed in the MCF10A-derived TrkA overexpression clones in the presence of NGF. Typically, the advancing front of cells as the wound closes migrate in a fairly regular fashion, resulting in a slightly ragged but relatively even edge. In the MCF10A TrkA-

overexpressing lines with NGF, the advancing lines were wavy and uneven, suggesting perhaps a difference in migration not otherwise observed (Figure 23).

Because an increased growth phenotype had already been observed in these cell lines, it was important to perform migration assays that were independent of growth, which the scratch assay is unable to fully separate. For this purpose, trypsinized MN or MEV cells were suspended in growth factor-free media separated from a well containing normal media containing NGF by microchannels of various widths. Time lapse imaging allowed the tracking of individual cells as they migrate up the chemotactic gradient. This produced measures of speed, persistence and velocity. Speed is here defined as the amount of movement an individual cell shows, independent of direction. Persistence quantifies the extent to which a cell continues to move across the channel, with a perfectly straight path from low growth factor media to high growth factor media having a value of 1. The product of these two quantities is the velocity, which reflects the migratory capacity of the cell.

In these assays, the speed of the TrkA overexpressors was observed to be double that of the empty vector control, reflecting a more motile cell (Figure 24). The persistence showed no significant difference (Figure 25). Velocity, the measure of migration, was significantly higher in the TrkA overexpressors as compared to the empty vector control (Figure 26). These assays were performed

in channels of varying widths from 3 uM to 20 uM. It was additionally observed that the TrkA overexpressors were more likely to enter the two smallest sets of channels, and so few cells entered these smallest channels for the empty vector control that these were impossible to accurately measure. The addition of the inhibitor larotrectinib had the effect of decreasing the speed and velocity measures, as well as causing the TrkA overexpressors to enter the smallest channels less frequently.

TrkA overexpression alters gene expression

Gene expression under growth arrest conditions in the presence of NGF were compared by microarray for one TrkA-overexpressing clone and the empty vector control of the MCF10A and hTERT-IMEC cell lines. Multiple genes were identified as being differentially expressed in both comparisons, listed in Tables 4 and 5. Of the genes listed, several have been identified in the literature as being involved in breast cancer tumorigenesis, metastasis, or progression. HIST1H2BM encodes a histone protein increased in breast cancer progression in the MCF10AT model (20). FEN1, flap endonuclease 1, is elevated in DNA damage, interacts with APC to promote breast cancer development, (21) and is associated with poor prognosis and highly aggressive tumor types (22). HSD17B2, hydroxysteroid 17b-dehydrogenase type 2, is modulated by estrogen

exposure (23), catalyzes conversion between estrogen forms, and is upregulated in ER-negative breast cancer (24). IL-1A, interleukin 1A, is involved in a pro-inflammatory feed-forward loop that promotes breast cancer tumorigenesis and chemotherapy resistance (25). FBXO45, F-box protein 45, is an E3 ubiquitin ligase that is involved in estrogen receptor degradation (26) and altering chemosensitivity (27). SFN, stratifin, is important to cellular movement and correlated with poor progression and aggressive breast cancer subtypes (28). ERCC6L, excision repair cross-complementation group 6 like, is a DNA helicase that promotes cell proliferation and survival in breast cancer (29). EFNB2, ephrin B2, is prognostic for poor breast cancer survival when cytoplasmic rather than membrane-bound (30), is a target of TGFb in pro-invasive and migratory processes (31), and modulates expression of metalloproteases MMP9 and MMP2 in these invasive processes (32). PLAGL2, pleomorphic adenoma gene like-2, is a zinc finger translational factor that promotes migration by interacting with the actin cytoskeleton (33). Of the downregulated genes, TSHZ2 is a zinc finger homeobox protein that releases tumorigenesis-promoting GLI1 when downregulated in breast cancer (34) and TSC22D3, glucocorticoid leucine zipper, is an apoptosis-regulating transcription factor downregulated by estrogen in breast cancer cells (35).

TrkA overexpression increases growth in a tumorigenic breast cell line *in vivo*

Initial assays in NOD-SCID mice indicated that the overexpression of TrkA does not confer tumorigenicity on the MCF10A cell line. Therefore, a TrkA-overexpression model was developed in the tumorigenic MCF7 cell line by the protocol described above in order to produce an *in vivo* model. Briefly, multiple isogenic TrkA-overexpressing clones as well as an empty vector control were produced by single-cell isolation of transfected MCF7 cells. Western blot was utilized to confirm overexpression of the TrkA protein as compared to the low but detectable level seen in the parental MCF7. In mice, TrkA overexpression conferred higher proliferation but did not confer estrogen independence (Figure 33). TrkA expression in the tumors was confirmed by immunohistochemistry. No gross metastases were observed. In the tumorigenic MCF7 cell line, TrkA overexpression increases proliferation *in vivo* but does not alter estrogen dependence or invasiveness.

TrkA overexpression confers the capacity for disseminated disease formation

The MCF7 cell lines were next interrogated by tail vein injection to determine the capacity for disseminated disease formation, an indicator of metastatic capacity. Whereas the parental MCF7 cell line does not form tumors when injected in the tail vain, the TrkA-overexpressing MCF7 cell lines formed

microscopic and macroscopic tumors in lung as well as salivary gland and other organs (Figures 34, 35).

Cell Line	*Description*
MCF10A	Parental MCF10A cell line
MEV	MCF10A expressing pIRESneo3 vector
MN1	MCF10A expressing *NTRK1*-pIRESneo3 vector
MN2	MCF10A expressing *NTRK1*-pIRESneo3 vector
MN3	MCF10A expressing *NTRK1*-pIRESneo3 vector
MN4	MCF10A expressing *NTRK1*-pIRESneo3 vector
hTERT-IMEC	Parental hTERT-IMEC cell line
HIpI	hTERT-IMEC expressing pIRESneo3 vector
HIN2	hTERT-IMEC expressing *NTRK1*-pIRESneo3 vector
HIN3	hTERT-IMEC expressing *NTRK1*-pIRESneo3 vector
HIN4	hTERT-IMEC expressing *NTRK1*-pIRESneo3 vector
HIN5	hTERT-IMEC expressing *NTRK1*-pIRESneo3 vector
CDN2	MCF10A expressing *CD74-NTRK1* translocation vector
CDN3	MCF10A expressing *CD74-NTRK1* translocation vector
CDN4	MCF10A expressing *CD74-NTRK1* translocation vector
MCF7	Parental MCF7 cell line
MCF7 EV	Parental MCF7 cell line expressing pIRESneo3 vector
MCF7 TrkA	MCF7 expressing *NTRK1*-pIRESneo3 vector

Table 1: Cell lines used in this study.

Primer Name	*Sequence*
R ntrk1 center	GCACTCAGCAAGGAAGACCT
F ntrk1 center	GGCAGAGGTCTCTGTTCAGG
R ntrk1 RC213091	TTGCTGCCAGATCCTCTTCT
F ntrk1 RC213091	GATCCGGTACCGAGGAGAT
NotI-ntrk1 R Long	CATTAGGCGGCCGCACCTAGGCCCAGGACATCC AGGTAGACAGGAGGTG
NotI-ntrk1 Reverse	CATTAGGCGGCCGCACCTAGGCCCAGGACATCC AGGTAGA
NotI-ntrk1 Forward	GATTACAGCGGCCGCACCATGCTGCGAGGCGGA CGGCG
NTRK1cDNA R2	TTGTCCATGAAGGCAGCCAT
NTRK1 cDNA F2	TGGTCTCATTGAGCACGGAG
NTRK1 cDNA R1	AATGGCTCCGTGCTCAATGA
NTRK1 cDNA F1	AGGGTTGTCCATGAAGGCAG
pIRES-MCS-ntrk1 R2	AACGCCACAGCATCAAGGAT
pIRES-MCS-ntrk1 F2	GTACTCACCCCAACAGCTGG
pIRES-MCS-ntrk1 R1	CAGCATCAAGGATGTGCACG
pIRES-MCS-ntrk1 F1	GGAGTACTCACCCCAACAGC

Table 2: Primers used in this study.

Study	Total Cases	*NTRK1* Amplified	Percent Amplified	Total TNBC	TNBC *NTRK1* Amplified	Percent Amplified
METABRIC	2051	436	21.26%	**-**	**-**	**-**
BCCRC Xenograft	29	4	13.79%	**-**	**-**	**-**
The MBC Project	103	13	12.62%	**-**	**-**	**-**
TCGA 2015	505	55	10.89%	5	1	20%
TCGA	963	102	10.59%	60	13	21.67%
Sickkids 2016	213	17	7.98%	-	-	-
TCGA Pub	482	22	4.98%	123	11	8.94%

Table 3: Frequency of *NTRK1* amplification in breast cancers via cBioPortal.

	Fold Change in MCF10A	*Fold Change in hTERT-IMEC*
HIST1H2BM	2.00E+05	4.09E+02
FEN1	1.31E+03	2.37E+01
SPINK6	8.70E+02	8.61E+00
HIST1H3I	7.29E+02	4.89E+01
GSG2	3.76E+02	2.76E+01
HIST1H2AG	1.73E+02	1.85E+01
CHAC2	1.56E+02	7.87E+00
HYLS1	1.16E+02	5.36E+00
HSD17B2	7.55E+01	7.35E+01
PIGW	6.42E+01	1.34E+01
HIST1H2BL	4.62E+01	1.48E+01
MT1G	3.55E+01	3.76E+00
IL1A	2.60E+01	3.05E+01
EEF1E1	2.19E+01	5.58E+00
PGP	1.81E+01	3.67E+00
HIST2H2AB	1.66E+01	2.82E+01
LLPH	1.52E+01	3.58E+00
TRIM59	1.21E+01	3.78E+00
FBXO45	1.17E+01	3.63E+00
HIST1H4L	1.12E+01	3.39E+01
MT1M	1.08E+01	3.90E+00
CEBPG	9.73E+00	3.37E+00
HAUS2	8.57E+00	7.09E+00
TMEM97	8.02E+00	1.91E+01
HIST1H2BO	7.86E+00	1.61E+01
C5orf30	7.79E+00	4.86E+01
SFN	7.47E+00	1.34E+01
HIST1H2BH	7.44E+00	1.77E+01
IFIT3	7.42E+00	1.33E+04
ERCC6L	7.24E+00	2.21E+01
EFNB2	6.42E+00	6.27E+00
C10orf12	5.58E+00	2.66E+01
TIFA	4.42E+00	6.47E+00
IER3	4.36E+00	3.88E+01
HIST1H2BE	4.20E+00	1.39E+01
CLIC1	4.13E+00	3.90E+00
HIST1H4C	4.02E+00	2.27E+01
MID1IP1	3.95E+00	3.24E+00
PLAGL2	3.21E+00	3.95E+00

Table 4: Genes upregulated in TrkA- overexpressors by microarray.

	Fold Change in MCF10A	*Fold Change in hTERT-IMEC*
PCDHB5	2.94E-01	1.18E-01
CBLN3	2.51E-01	1.50E-01
TACSTD2	2.50E-01	8.87E-02
IRX5	2.25E-01	2.25E-01
PCDHB3	2.10E-01	2.40E-01
DIRC1	1.86E-01	1.31E-01
FAM229B	1.81E-01	1.35E-01
RWDD2A	1.70E-01	2.64E-01
TMEM127	1.66E-01	2.57E-01
MB21D2	1.62E-01	1.74E-01
PCDHB16	1.52E-01	1.84E-03
GJA5	1.43E-01	1.50E-01
TCEAL3	1.39E-01	2.49E-01
GPR1	1.22E-01	9.37E-03
PCDHB10	7.48E-02	9.70E-02
TSHZ2	6.99E-02	2.85E-01
TSC22D3	4.25E-03	4.21E-02
CITED2	7.07E-05	2.98E-01

Table 5: Genes downregulated in TrkA-overexpressors by microarray.

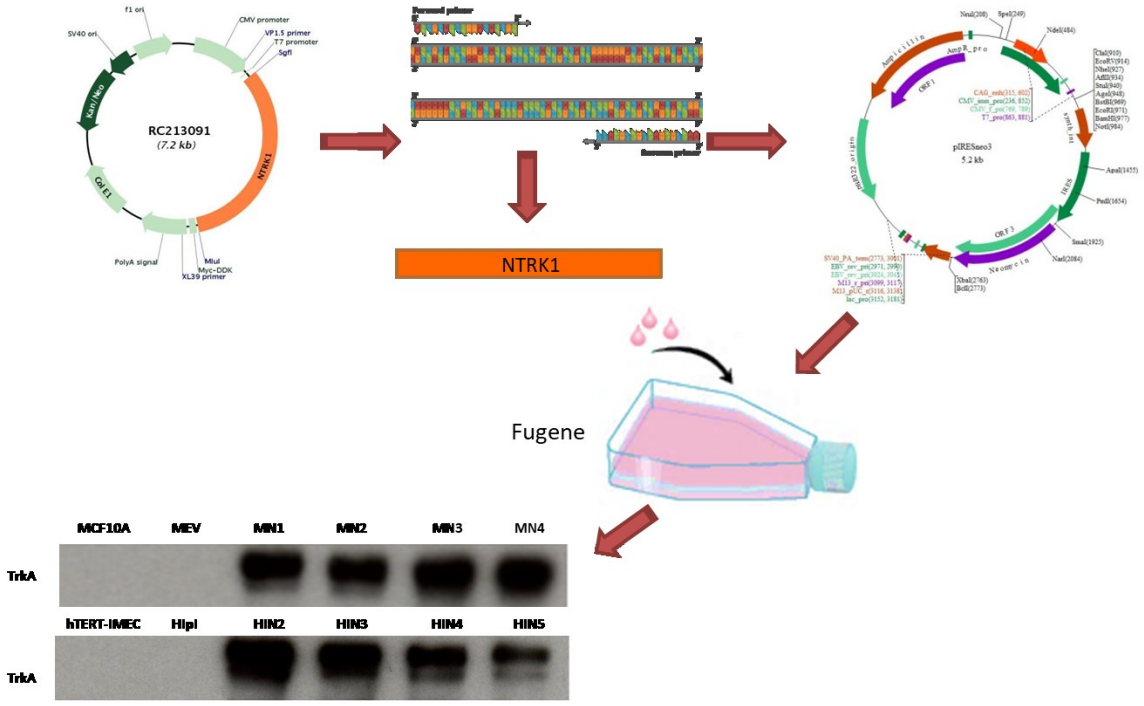

Figure 1: Experimental design. *NTRK1* cDNA was isolated by PCR from RC213091 vector and ligated to pIRESneo3 vector, transfected using Fugene reagents, and multiple independent clones isolated in MCF10A and hTERT-IMEC parental cell lines.

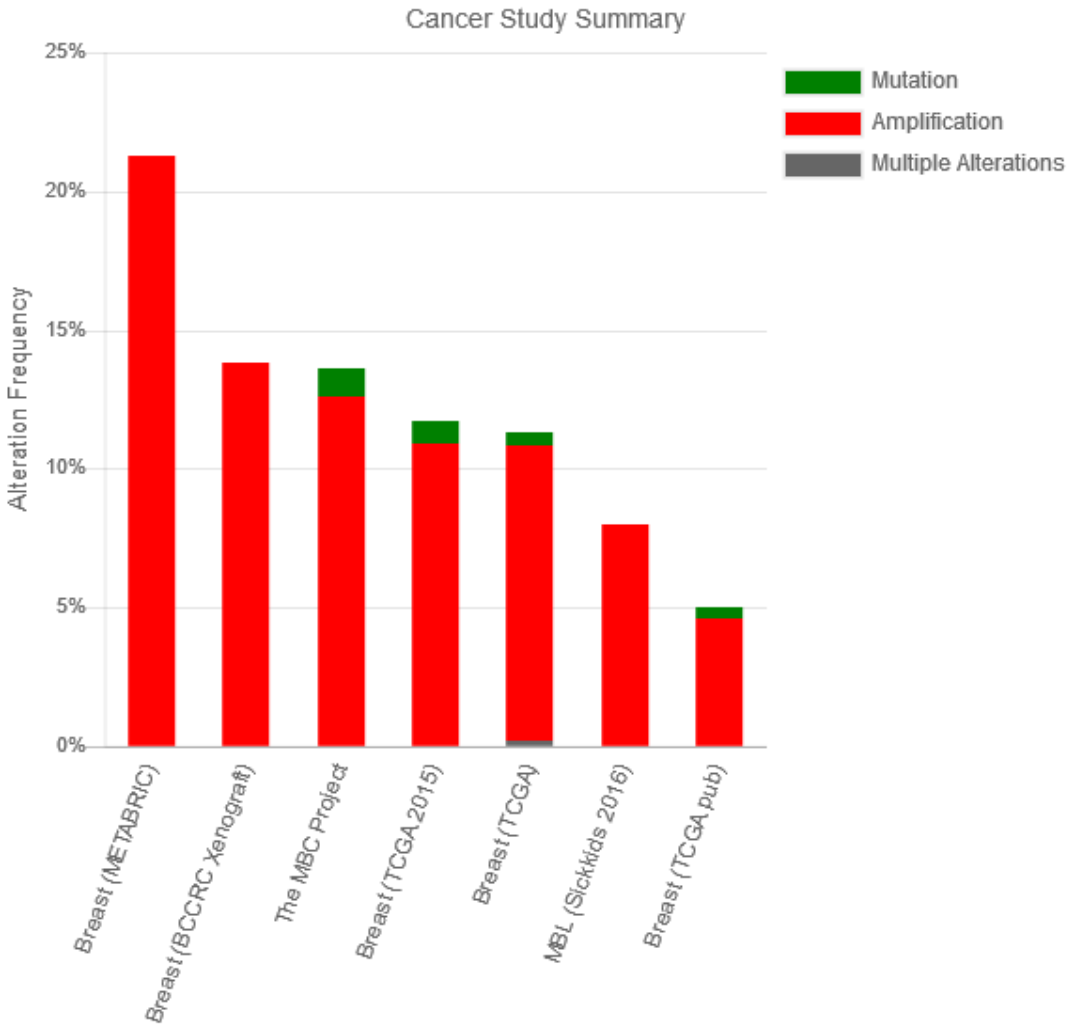

Figure 2: TrkA alterations across breast cancer studies as found in TCGA data via cBioPortal database. The primary alteration is amplification, in 5-22% of cases.

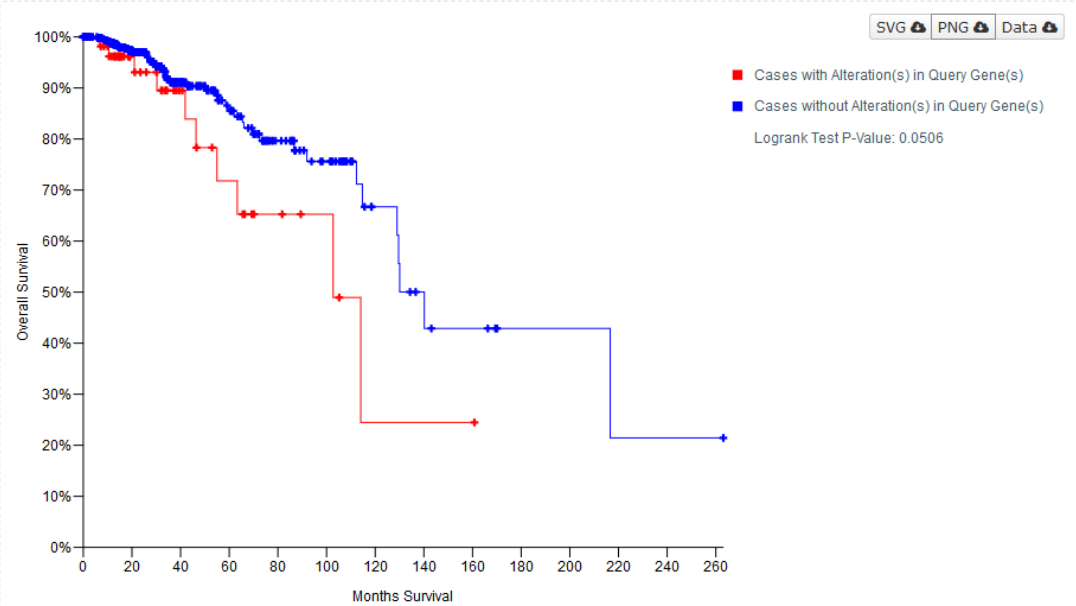

	Number of Cases, Total	Number of Cases, Deceased	Median Months Survival
Cases with Alteration(s) in Query Gene(s)	**59**	**10**	**102.69**
Cases without Alteration(s) in Query Gene(s)	**444**	**43**	**140.18**

Figure 3: Kaplan-Meier survival curves in breast invasive carcinoma, TCGA data, Cell 2015 dataset for breast cancers with GISTIC putative copy number alteration. In this data, alteration in TrkA confers a 40 month survival disadvantage.

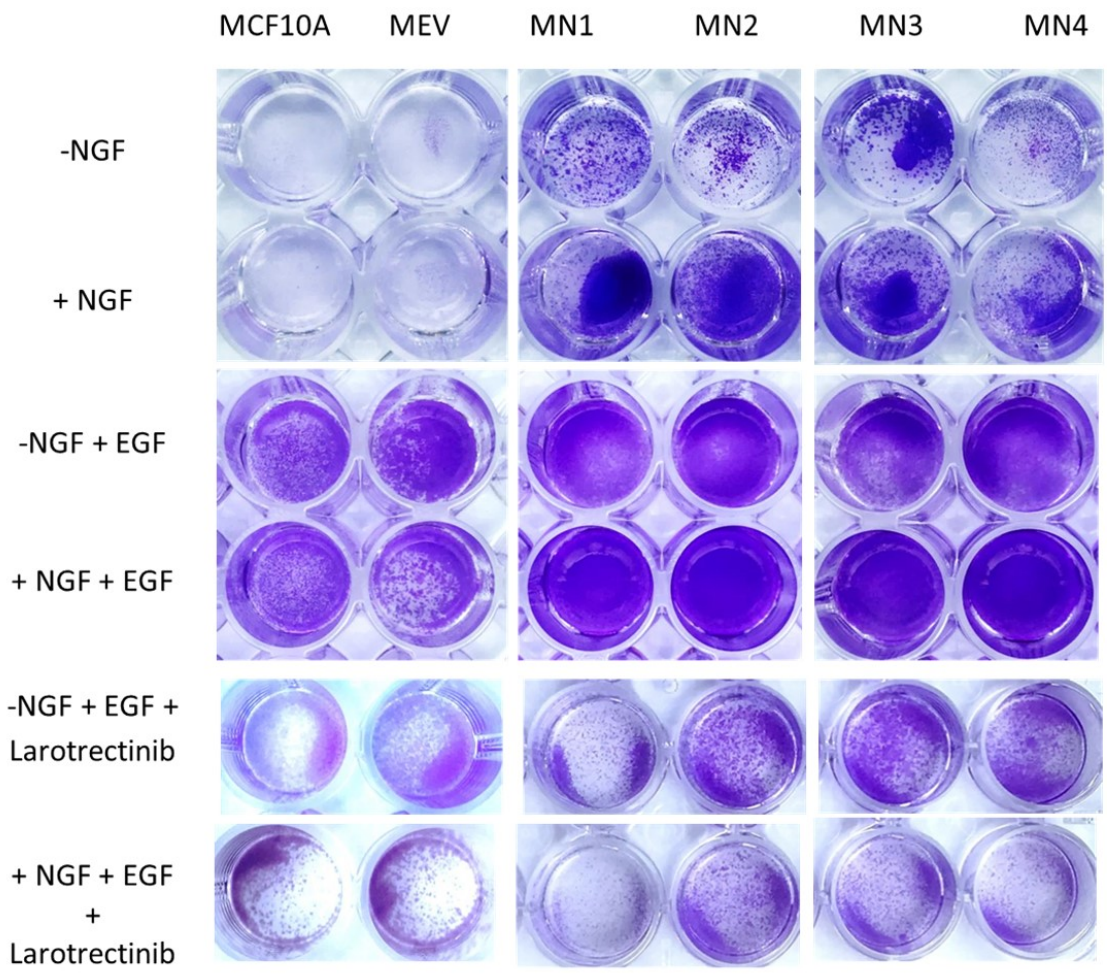

Figure 4: Parental MCF10A, empty vector control MEV and TrkA-overexpressing clones MN1-4 plated at 30,000 cells/well in 24-well plates, changed to the specified media at 24 hours, and stained with crystal violet at 5 days. Images taken from larger plates in smaller groups to avoid parallax effect. MCF10A arrest media, epidermal growth factor (EGF) added at 0.2 ng/mL, neuronal growth factor (NGF) added at 100 ng/mL and larotrectinib added at 1.5uM as specified.

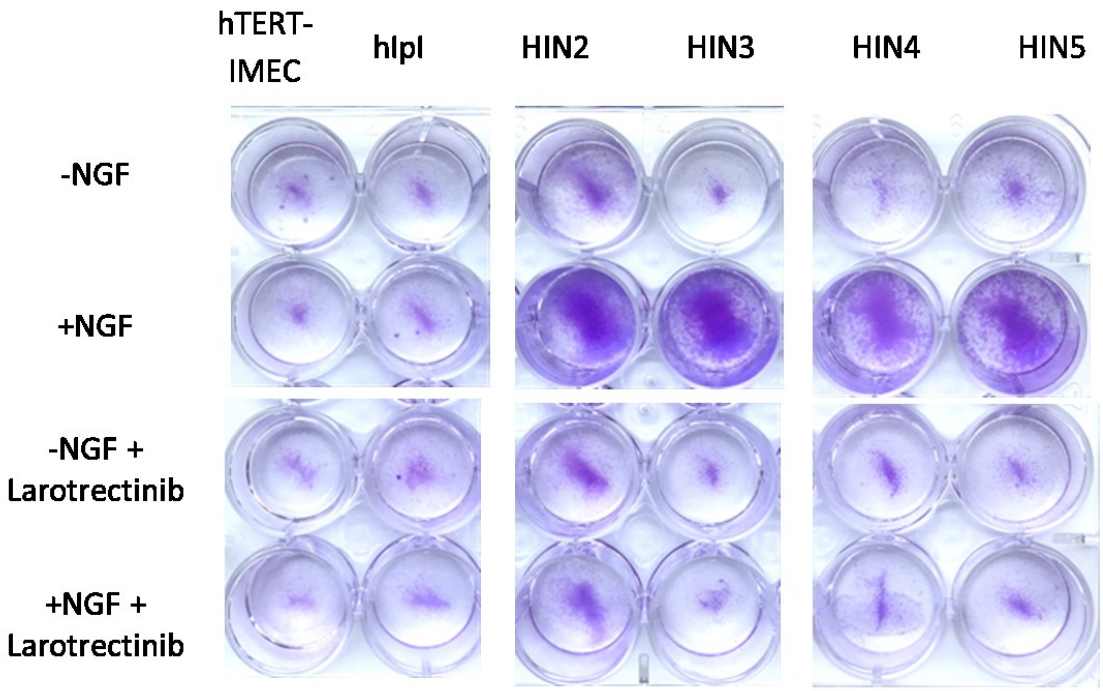

Figure 5: Parental hTERT-IMEC, empty vector control hIpI and TrkA-overexpressing clones HIN2-5 plated at 30,000 cells/well in 24-well plates, changed to the specified media at 24 hours, and stained with crystal violet at 5 days. hTERT-IMEC arrest media, neuronal growth factor (NGF) added at 12.5 ng/mL and larotrectinib added at 1.5uM as specified.

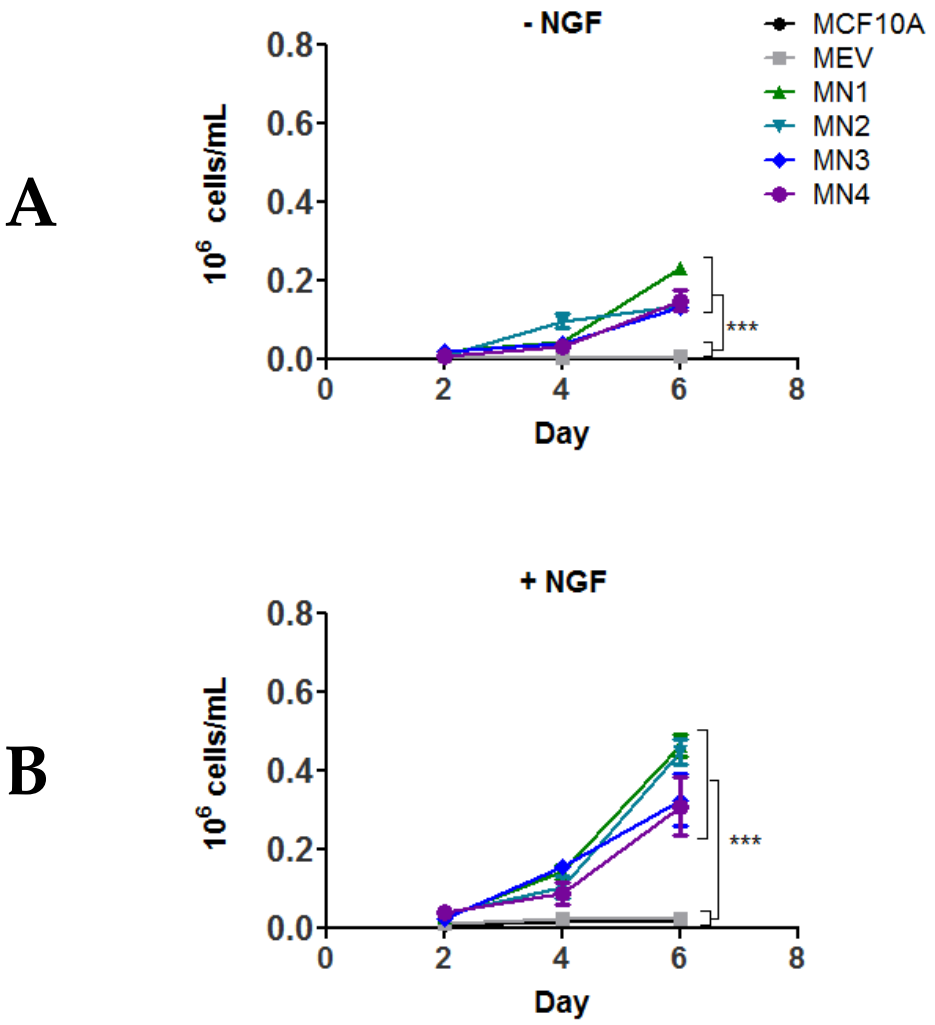

Figure 6: Parental MCF10A, empty vector control MEV and TrkA-overexpressing clones MN1-4 plated at 30,000 cells/well in triplicate in 24-well plates, changed to the specified media at 24 hours, and counted with a Beckman-Coulter cell counter at 2, 4, and 6 days. Mean ± SEM shown, ** $P \leq 0.001$, NS = not significant by ANOVA at 6 day time point. (A) Proliferation averages, arrest media alone (B) Proliferation averages, arrest media with neuronal growth factor, 100ng/mL.

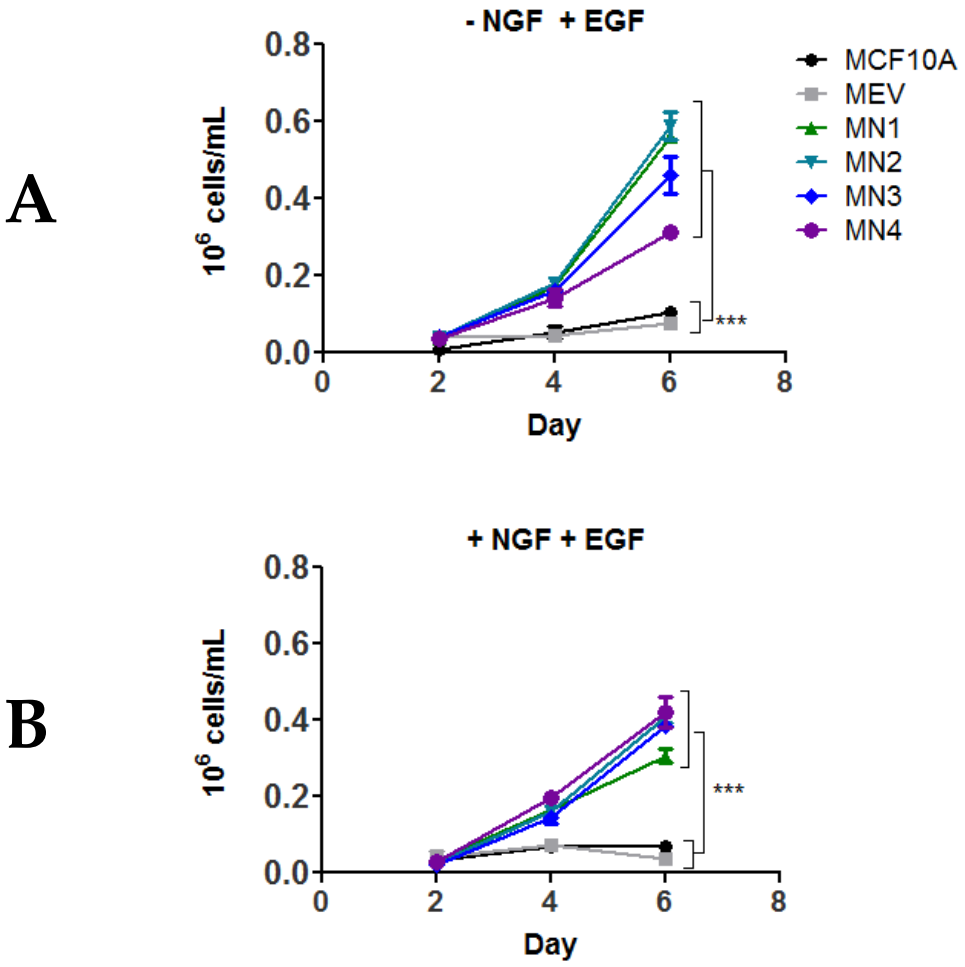

Figure 7: Parental MCF10A, empty vector control MEV and TrkA overexpressing clones MN1-4 plated at 30,000 cells/well in triplicate in 24-well plates, changed to the specified media at 24 hours, and counted with a Beckman-Coulter cell counter at 2, 4, and 6 days. Mean ± SEM shown, ** $P \leq 0.001$, NS = not significant by ANOVA at 6 day timepoint. (A) Proliferation averages, arrest media with physiologic levels of epidermal growth factor (EGF) at 0.2 ng/mL (B) Proliferation averages, arrest media with physiologic levels of epidermal growth factor (EGF) at 0.2 ng/mL, neuronal growth factor (NGF) added at 100 ng/mL.

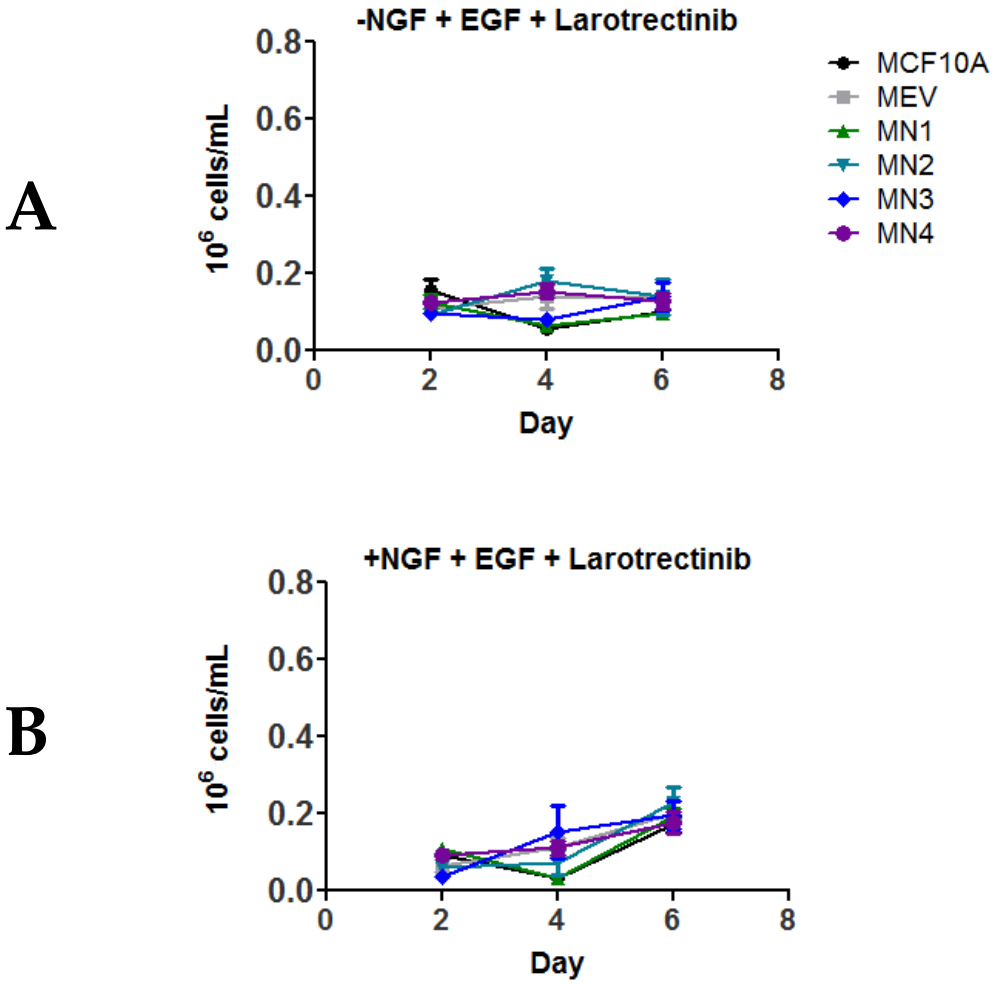

Figure 8: Parental MCF10A, empty vector control MEV and TrkA overexpressing clones MN1-4 plated at 30,000 cells/well in triplicate in 24-well plates, changed to the specified media at 24 hours, and counted with a Beckman-Coulter cell counter at 2, 4, and 6 days. Mean ± SEM shown, ** $P \leq 0.001$, NS = not significant by ANOVA at 6 day time point. (A) Proliferation averages, arrest media with physiologic levels of epidermal growth factor (EGF) at 0.2 ng/mL and larotrectinib, 1.5uM (B) Proliferation averages, arrest media with physiologic levels of epidermal growth factor (EGF) at 0.2 ng/mL, neuronal growth factor (NGF) added at 100 ng/mL, larotrectinib 1.5uM.

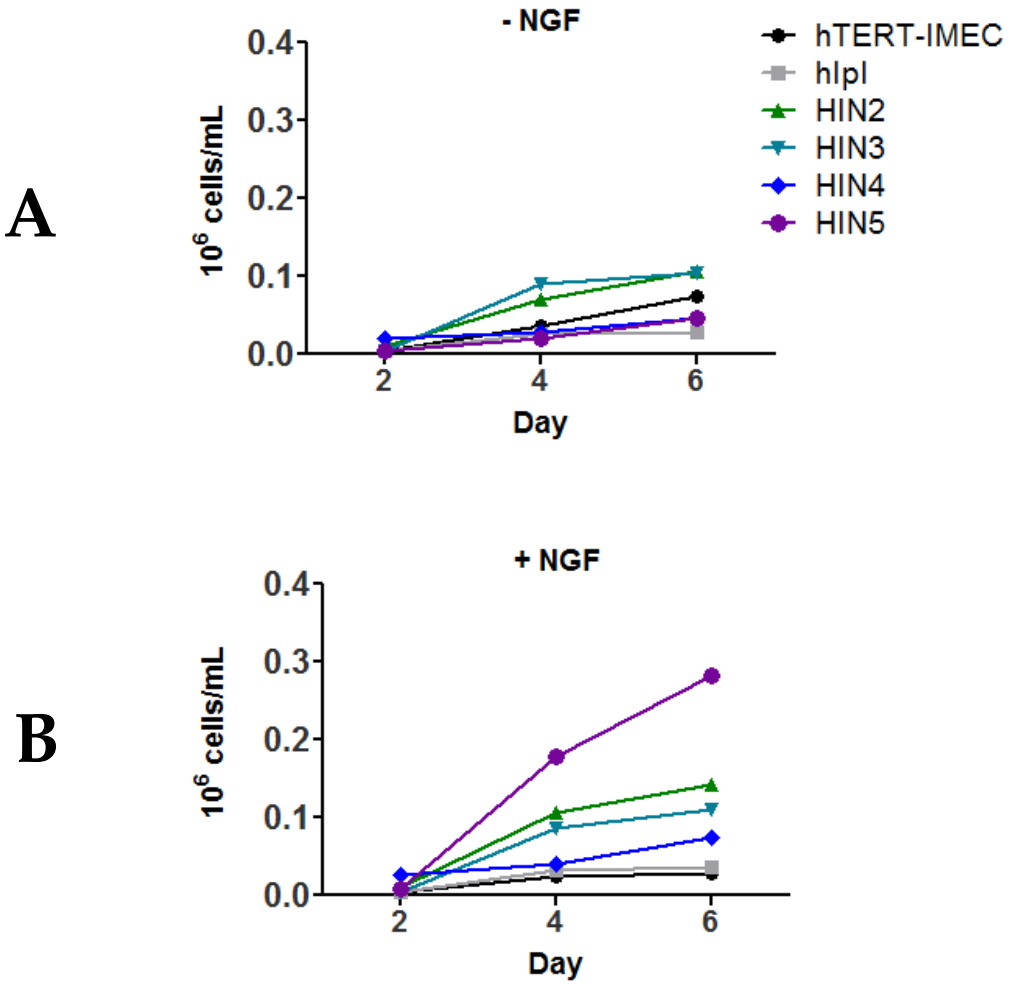

Figure 9: Parental hTERT-IMEC, empty vector control hIpI and TrkA overexpressing clones HIN2-5 plated at 30,000 cells/well in triplicate in 24-well plates, changed to the specified media at 24 hours, and counted with a Beckman-Coulter cell counter at 2, 4, and 6 days. Mean ± SEM shown, ** $P \leq 0.001$, NS = not significant by ANOVA at 6 day time point. (A) Proliferation averages, arrest media (B) Proliferation averages, arrest media with neuronal growth factor (NGF) added at 12.5 ng/mL.

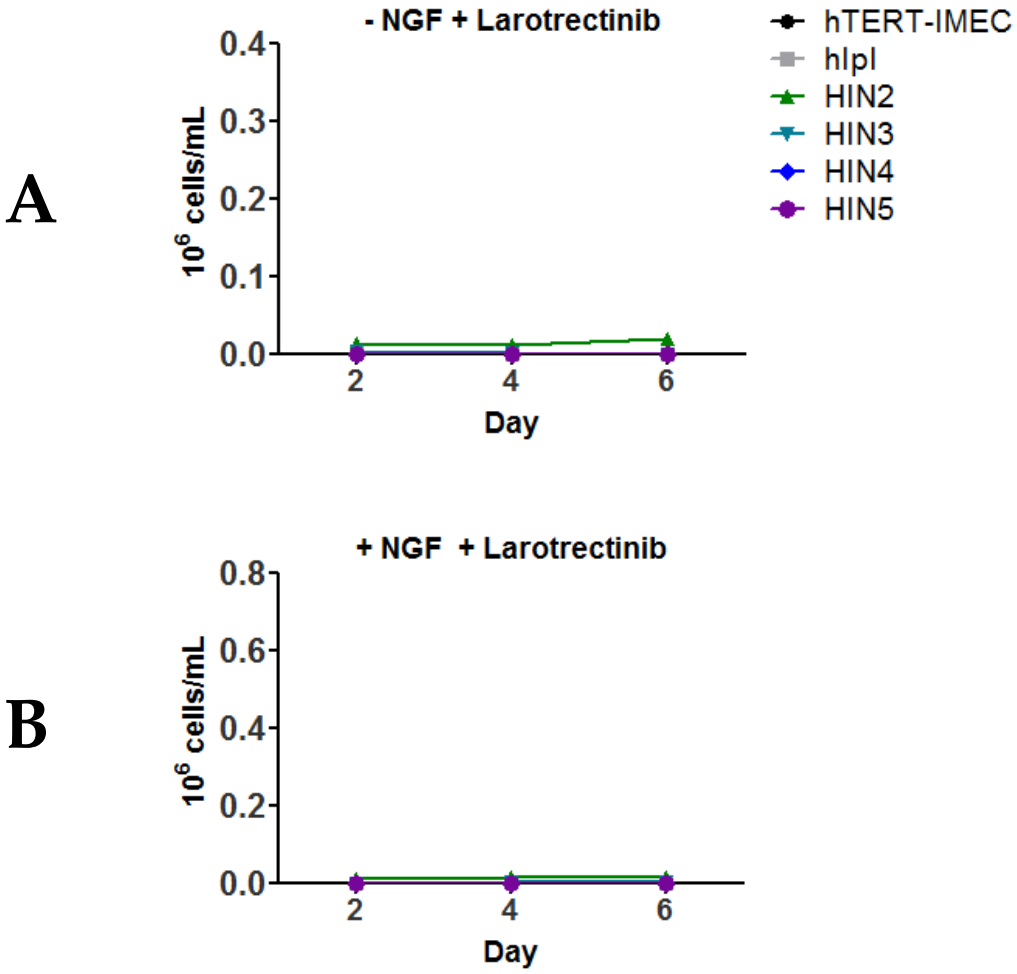

Figure 10: Parental hTERT-IMEC, empty vector control hIpI and TrkA overexpressing clones HIN2-5 plated at 30,000 cells/well in triplicate in 24-well plates, changed to the specified media at 24 hours, and counted with a Beckman-Coulter cell counter at 2, 4, and 6 days. Mean ± SEM shown, **P ≤ 0.001, NS = not significant by ANOVA at 6 day time point. (A) Proliferation averages, arrest media with larotrectinib, 1.5uM (B) Proliferation averages, arrest media with larotrectinib 1.5 uM, neuronal growth factor (NGF) added at 12.5 ng/mL.

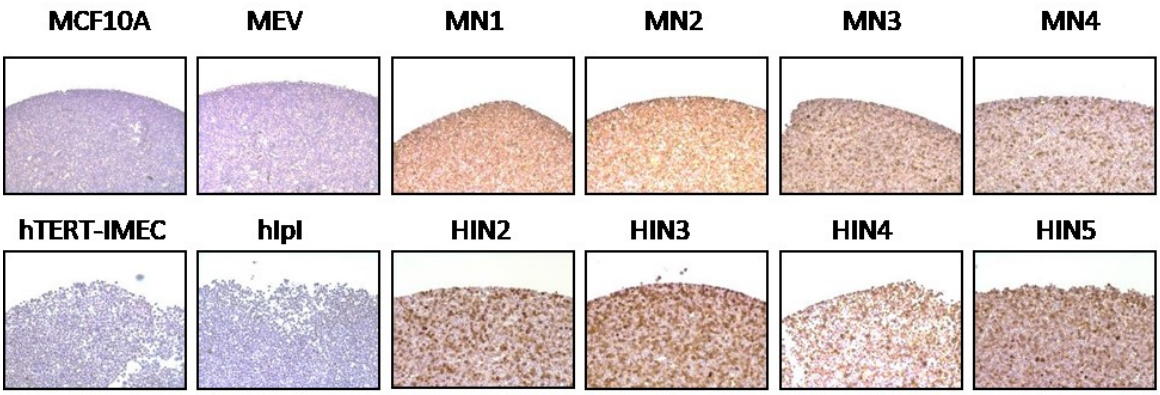

Figure 11: TrkA is expressed externally in overexpression cell lines (MN1-4, HIN2-5) and not in parental (MCF10A, hTERT-IMEC) or empty vector controls (MEV, hIpI). Cell pellets were fixed, sectioned, and stained with anti-TrkA antibody by immunohistochemistry.

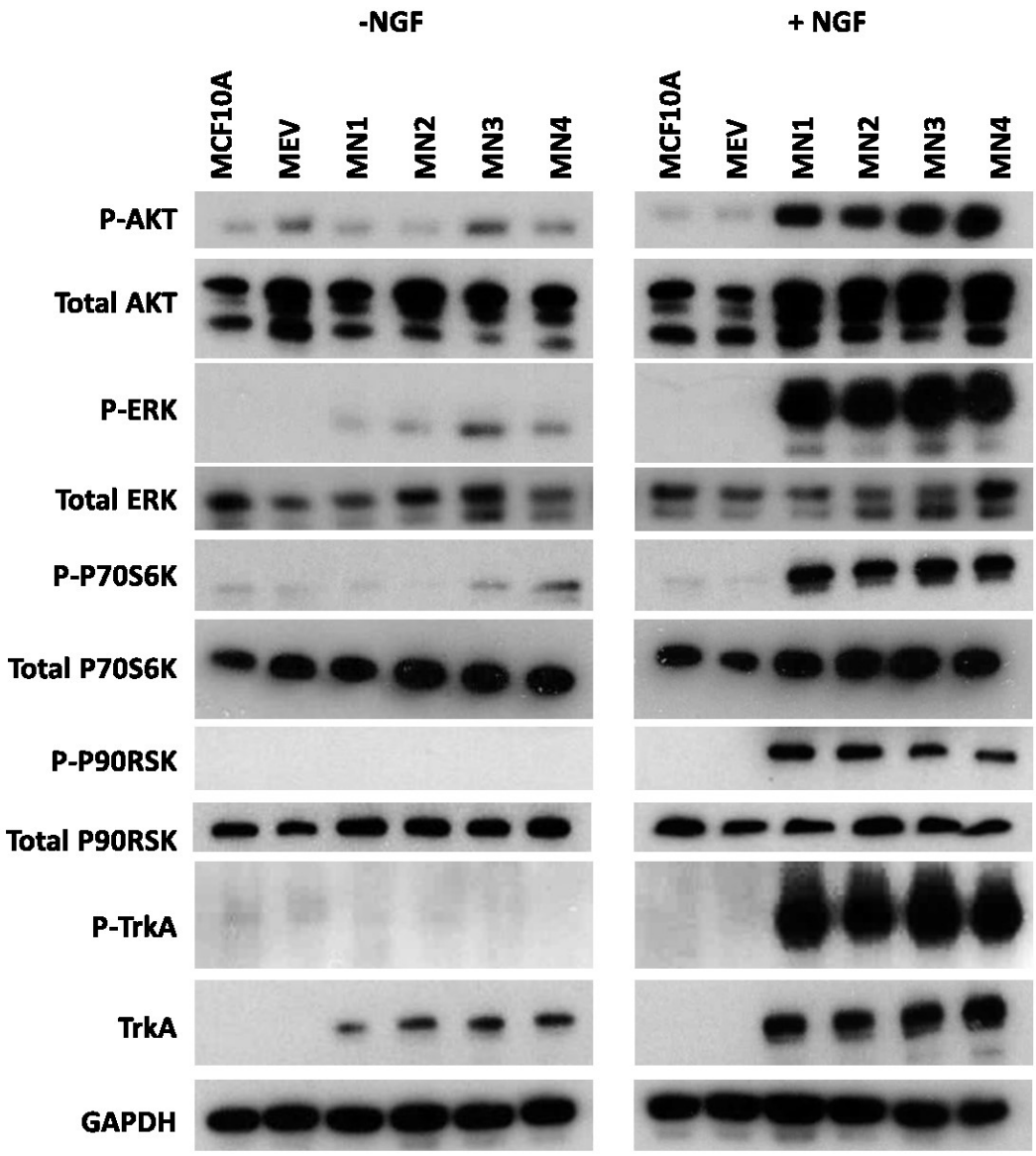

Figure 12: Western blots show activation in growth and survival pathways in TrkA overexpression lines, which is amplified with the addition of NGF and can be blocked with the inhibitor larotrectinib. Protein lysates for parental MCF10A, empty vector control MEV and TrkA overexpressing clones MN1-4 were collected after 24 hour exposure to arrest media conditions with and without NGF at 100ng/mL and subjected to western blot analysis with the indicated antibodies.

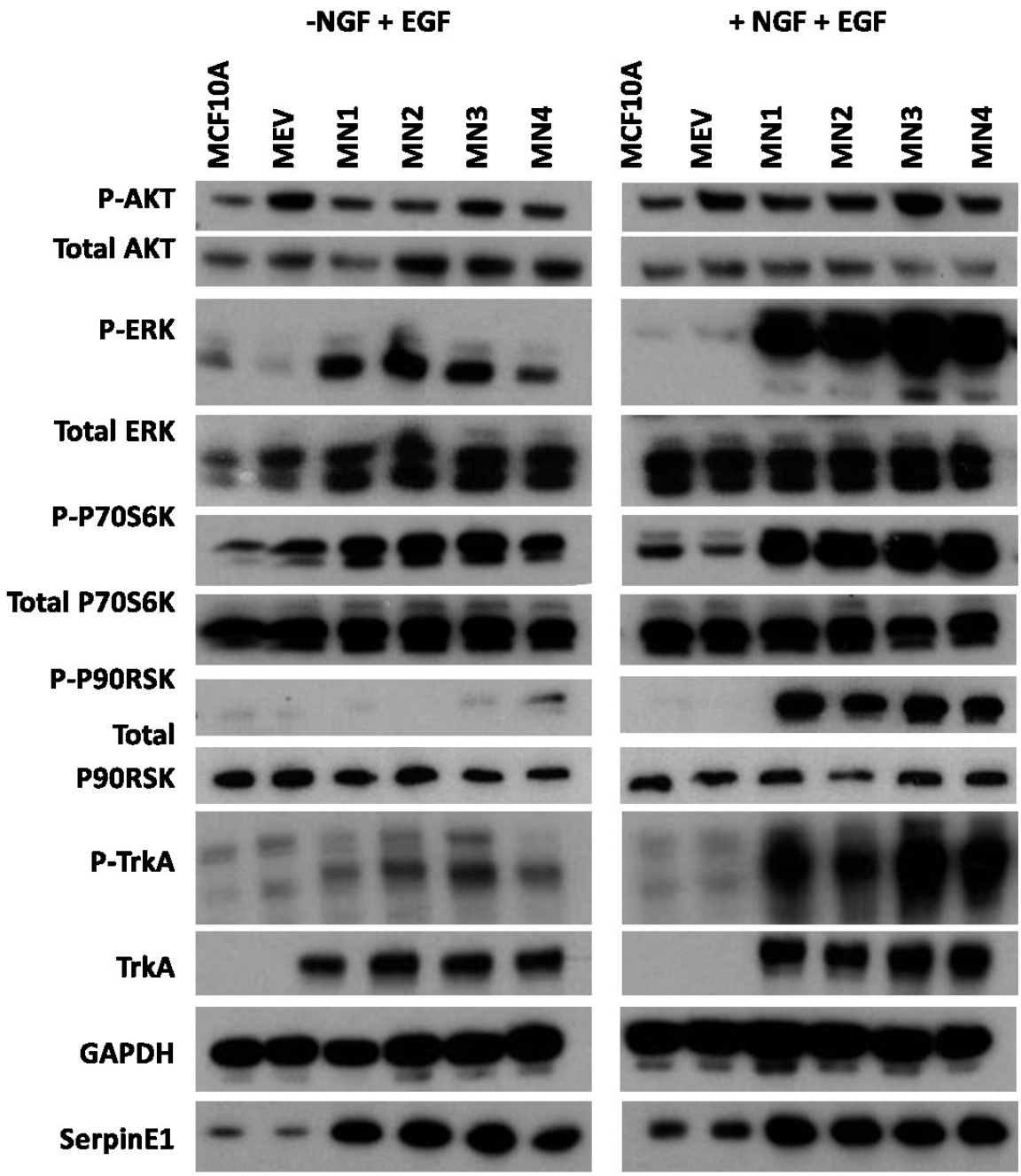

Figure 13: Protein lysates for parental MCF10A, empty vector control MEV and TrkA overexpressing clones MN1-4 were collected after 24 hour exposure to arrest media conditions supplemented with EGF at 0.2ng/mL with and without NGF at 100ng/mL and subjected to western blot analysis with the indicated antibodies.

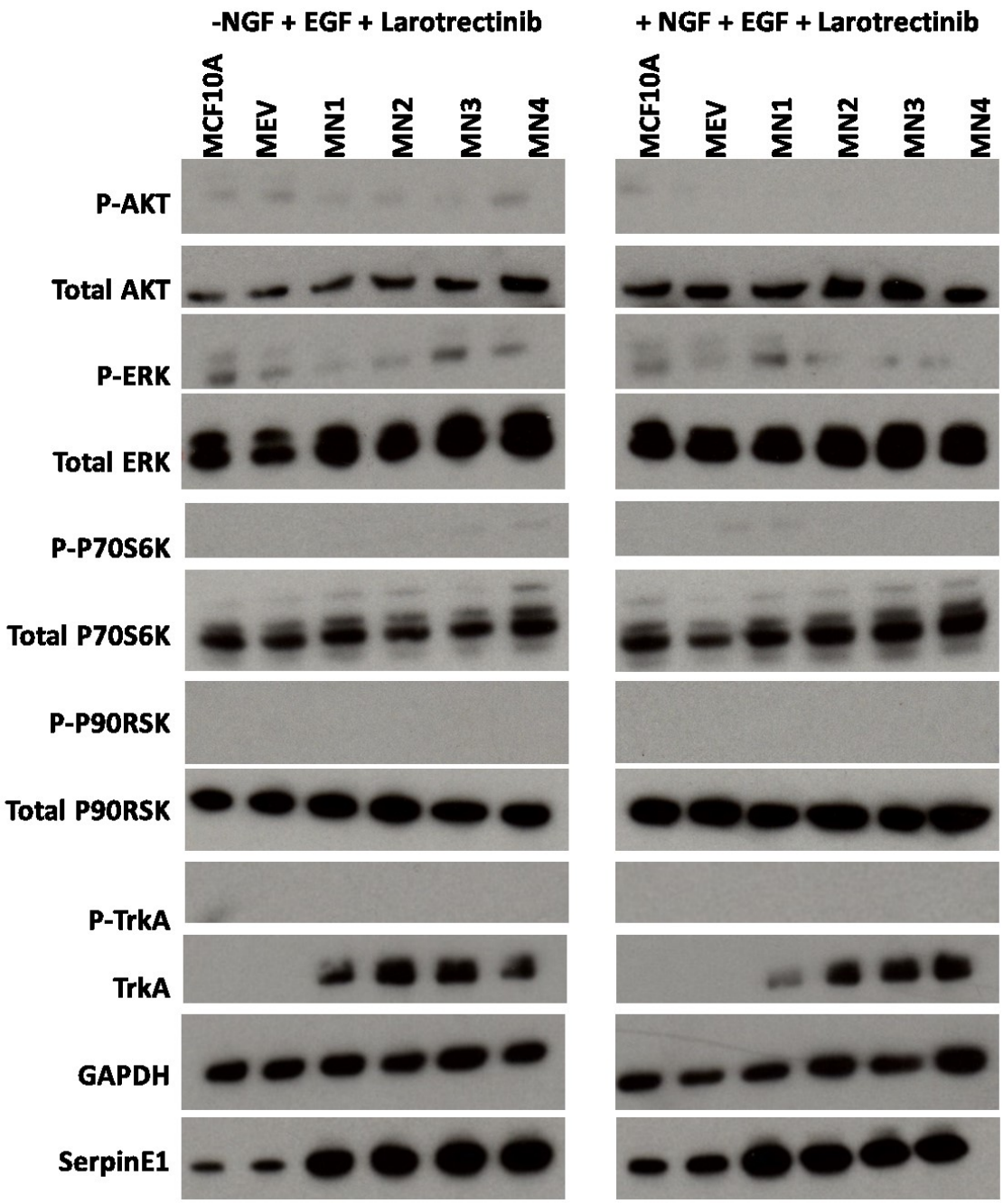

Figure 14: Protein lysates for parental MCF10A, empty vector control MEV and TrkA overexpressing clones MN1-4 were collected after 24 hour exposure to arrest media conditions supplemented with EGF at 0.2ng/mL and larotrectinib at 1.5uM, with and without NGF at 100ng/mL and subjected to western blot analysis with the indicated antibodies.

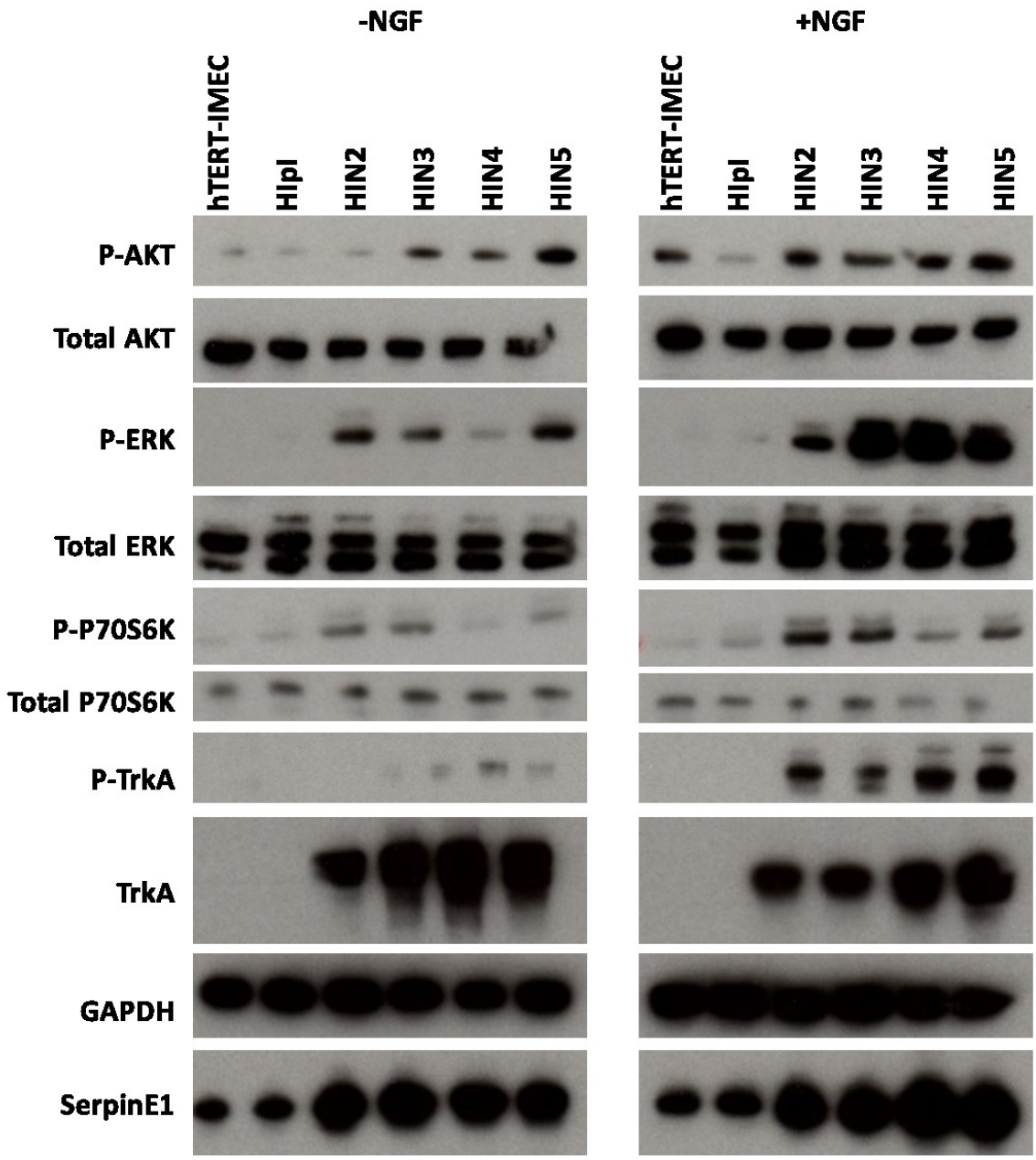

Figure 15: Protein lysates for parental hTERT-IMEC, empty vector control hIpI and TrkA overexpressing clones HIN2-5 were collected after 24 hour exposure to arrest media conditions with and without NGF at 12.5ng/uL and subjected to western blot analysis with the indicated antibodies.

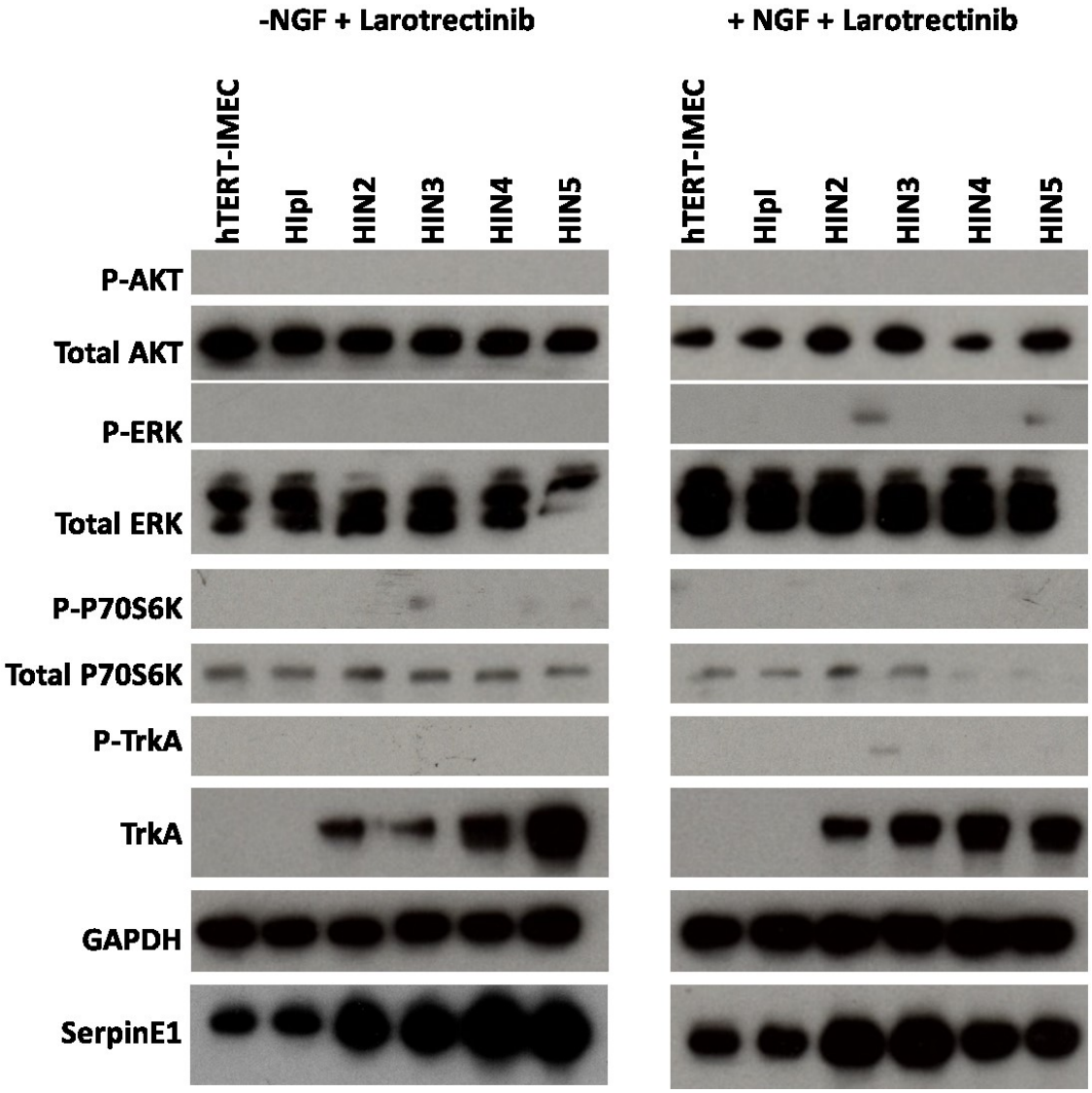

Figure 16: Protein lysates for parental hTERT-IMEC, empty vector control hIpI and TrkA overexpressing clones HIN2-5 were collected after 24 hour exposure to arrest media conditions with larotrectinib at 1.5uM, with and without NGF at 12.5ng/uL and subjected to western blot analysis with the indicated antibodies.

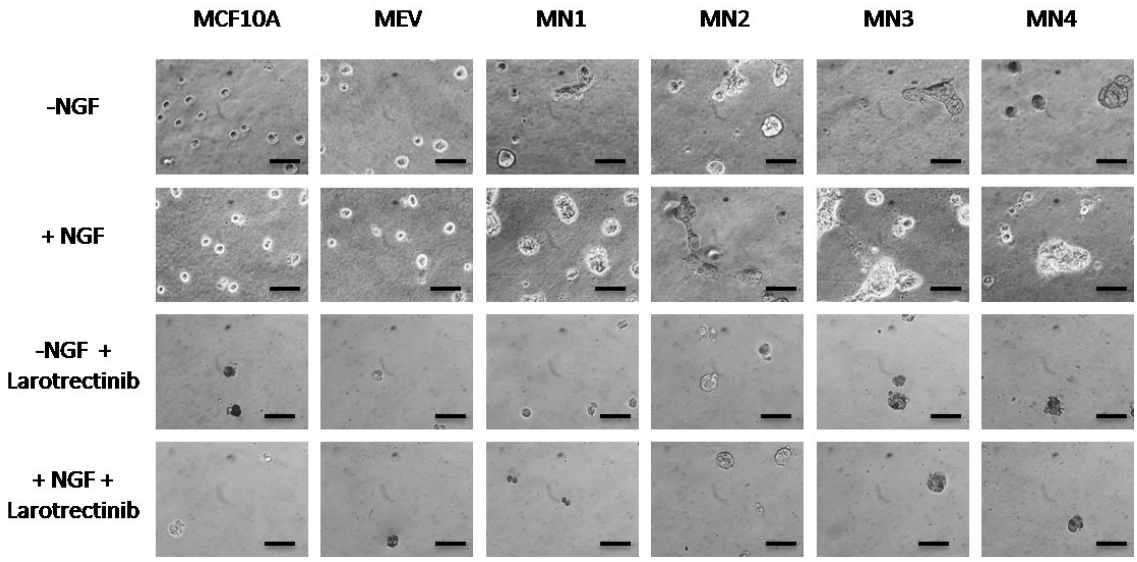

Figure 17: TrkA overexpression changes morphology and increases anchorage independent growth in three-dimensional culture. Parental MCF10A, empty vector control MEV and TrkA overexpressing clones MN1-4 were cultured in low growth factor conditions at low density in Matrigel under specified conditions. TrkA overexpressing clones showed larger, more irregular and spiculated colonies, exacerbated by neuronal growth factor (NGF) and reversed by larotrectinib. (Scale bar, 50 μm).

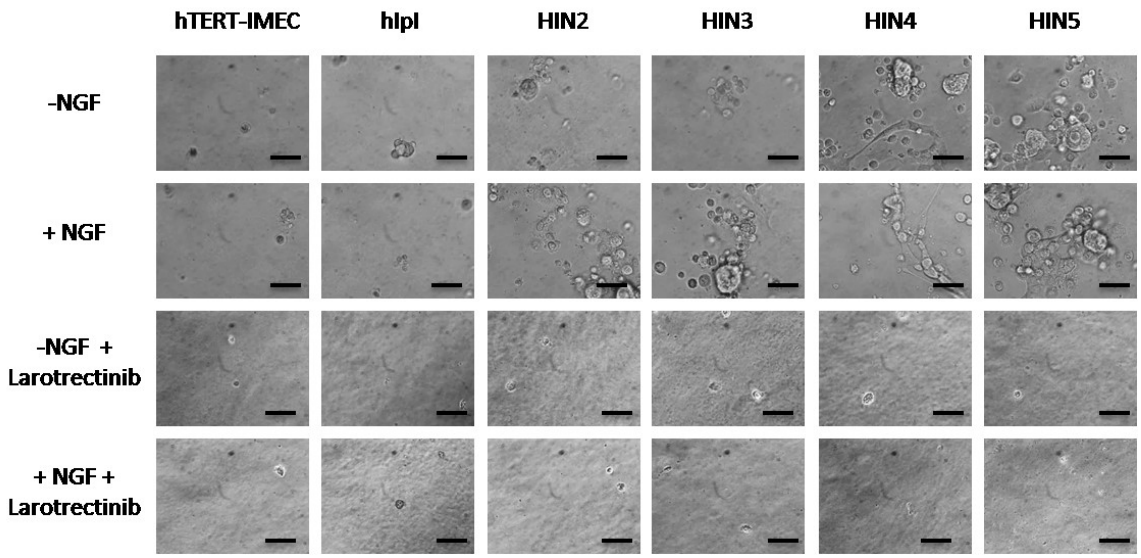

Figure 18: Parental hTERT-IMEC, empty vector control hIpI and TrkA overexpressing clones HIN2-5 were cultured in low growth factor conditions at low density in Matrigel under conditions specified. TrkA overexpressing clones showed larger, more irregular and spiculated colonies, exacerbated by neuronal growth factor (NGF) and reversed by larotrectinib. (Scale bar, 50 μm).

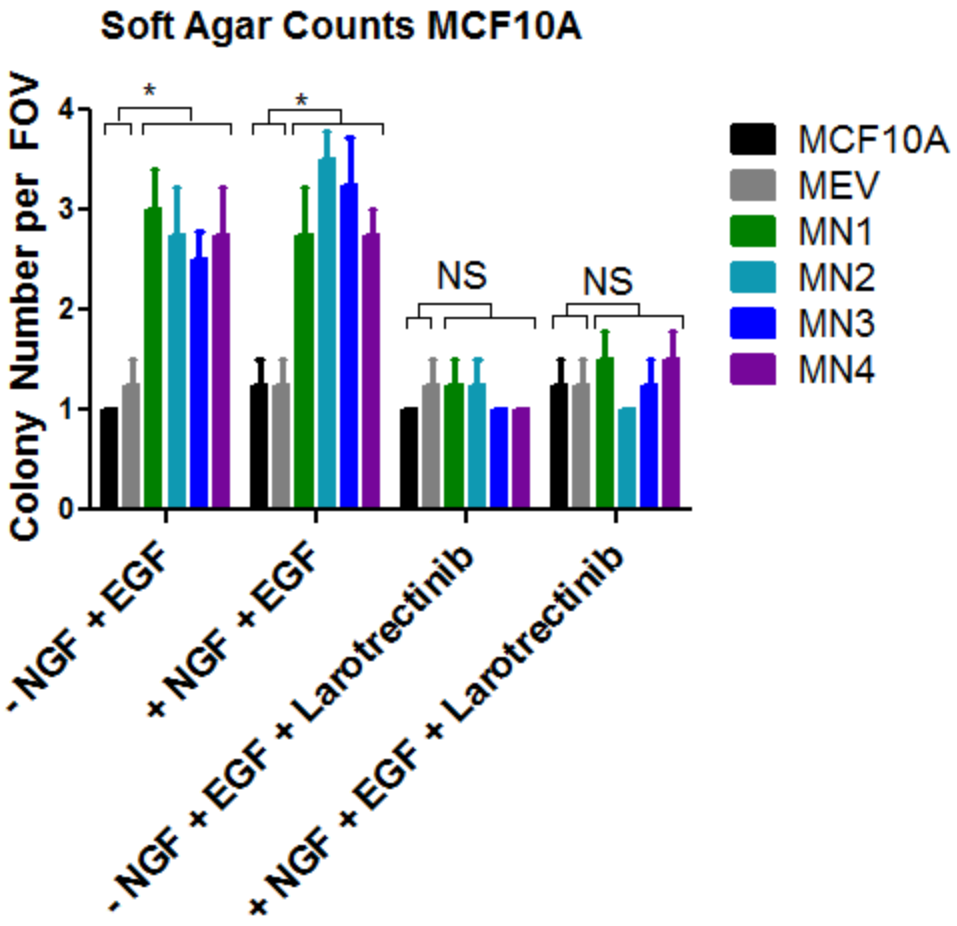

Figure 19: Parental MCF10A, empty vector MEV and TrkA overexpressing clones MN1-4 were cultured in low growth factor conditions at low density in 0.8% agar for two weeks, stained with crystal violet and imaged in multiple fields of view for colony quantification. TrkA overexpressing clones formed more colonies per field of view (FOV), increased by NGF and reduced by larotrectinib. Mean ± SEM shown, ** $P \leq 0.001$, NS = not significant by ANOVA.

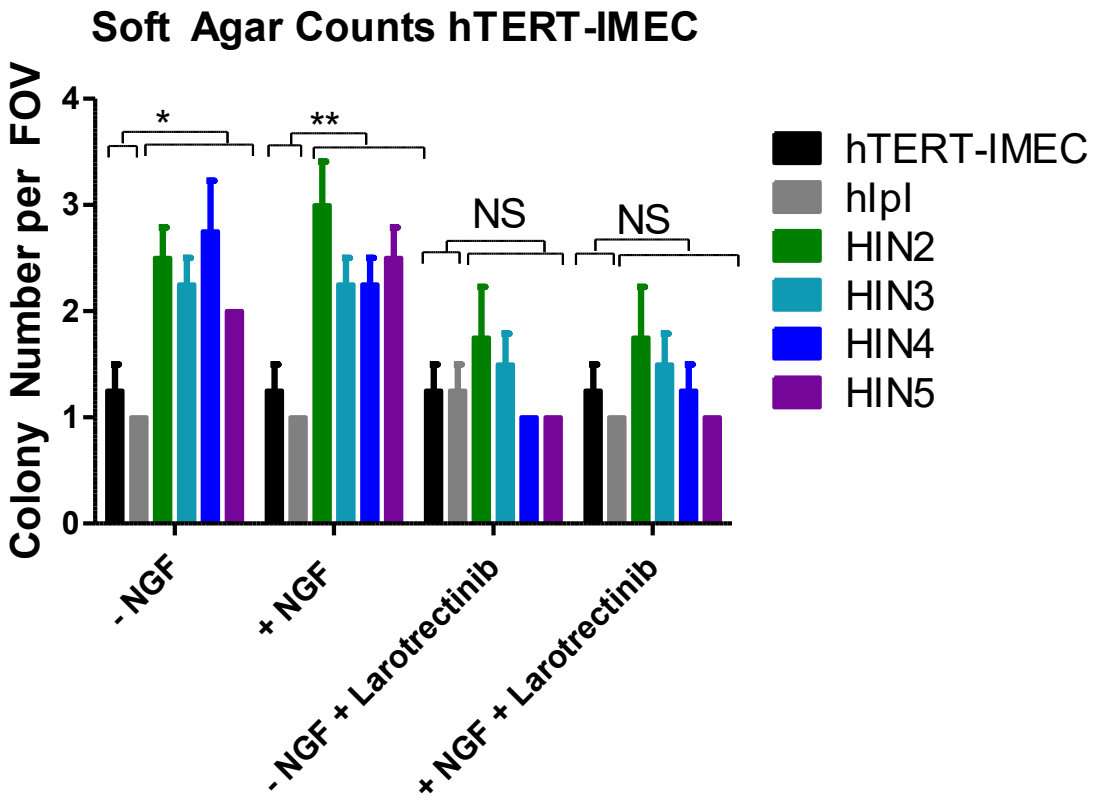

Figure 20: Parental hTERT-IMEC, empty vector hIpI and TrkA overexpressing clones HN2-5 were cultured in low growth factor conditions at low density in 0.8% agar for two weeks, stained with crystal violet and imaged in multiple fields of view for colony quantification. TrkA overexpressing clones formed more colonies per field of view (FOV), increased by NGF and reduced by larotrectinib. Mean ± SEM shown, ** $P \leq 0.001$, NS = not significant by ANOVA.

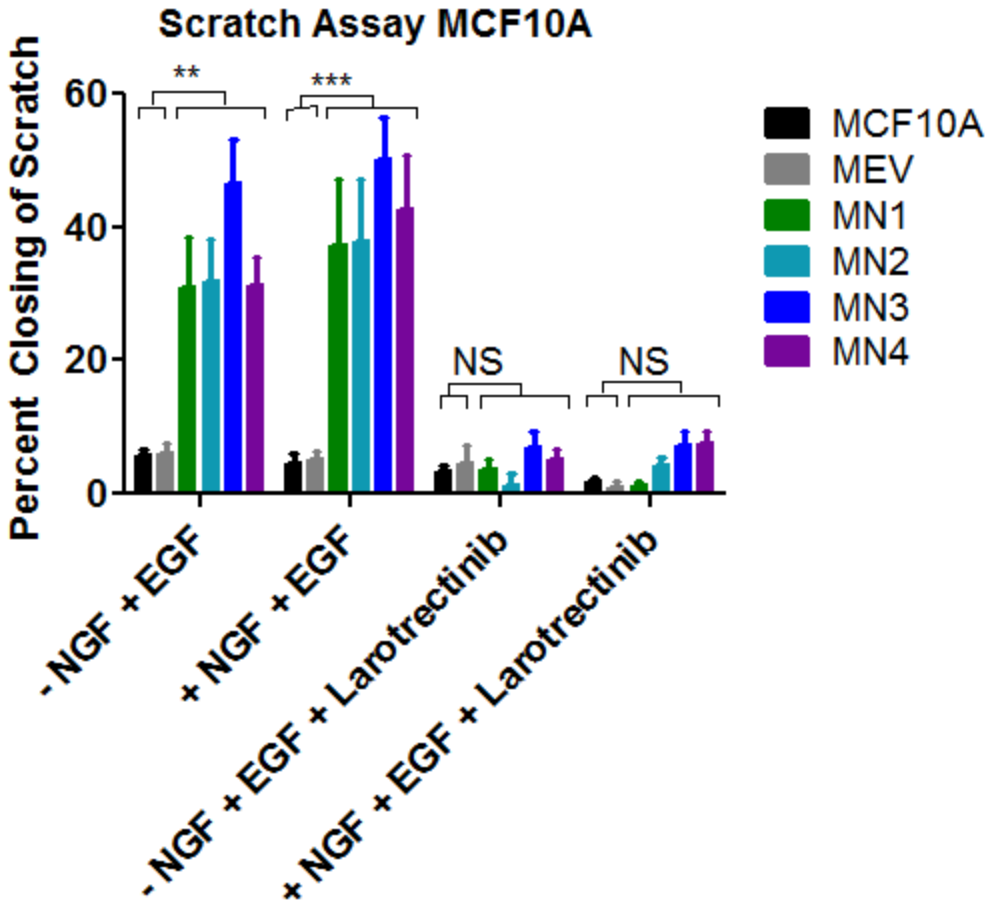

Figure 21: TrkA overexpression confers a migration advantage and changes wound healing morphology in MCF10A. Parental MCF10A, empty vector control MEV and TrkA overexpressing clones MN1-4 were plated to a confluent monolayer, scratched, and imaged at 0 and 16 hour time points; percent healing calculated from scratch dimensions quantified with ImageJ MiToBo software. TrkA overexpression confers higher wound healing especially with TrkA ligand neuronal growth factor (NGF) and larotrectinib inhibits this advantage.

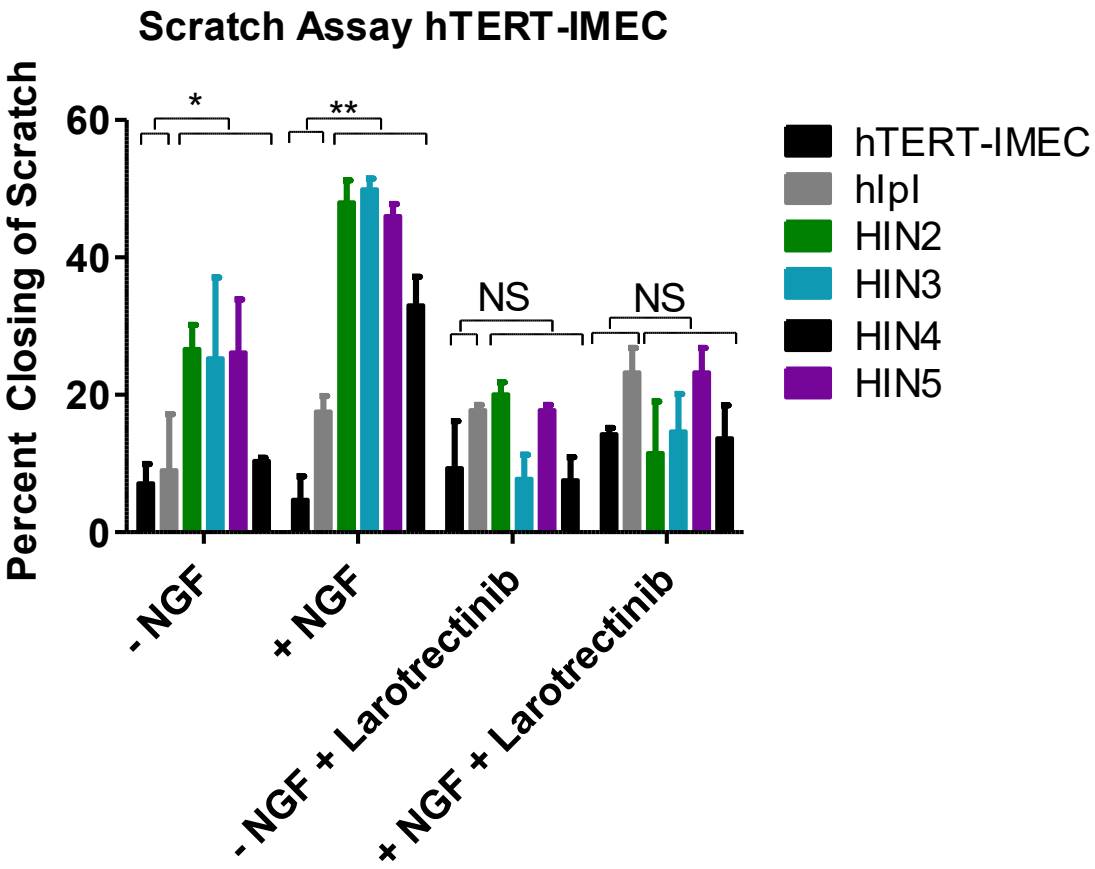

Figure 22: Parental hTERT-IMEC, empty vector control hIpI and TrkA overexpressing clones HIN2-5 plated to a confluent monolayer, scratched, and imaged at 0 and 16 hour time points; percent healing calculated from scratch dimensions quantified with ImageJ MiToBo software. TrkA overexpression confers higher wound healing especially with TrkA ligand neuronal growth factor (NGF) and larotrectinib inhibits this advantage.

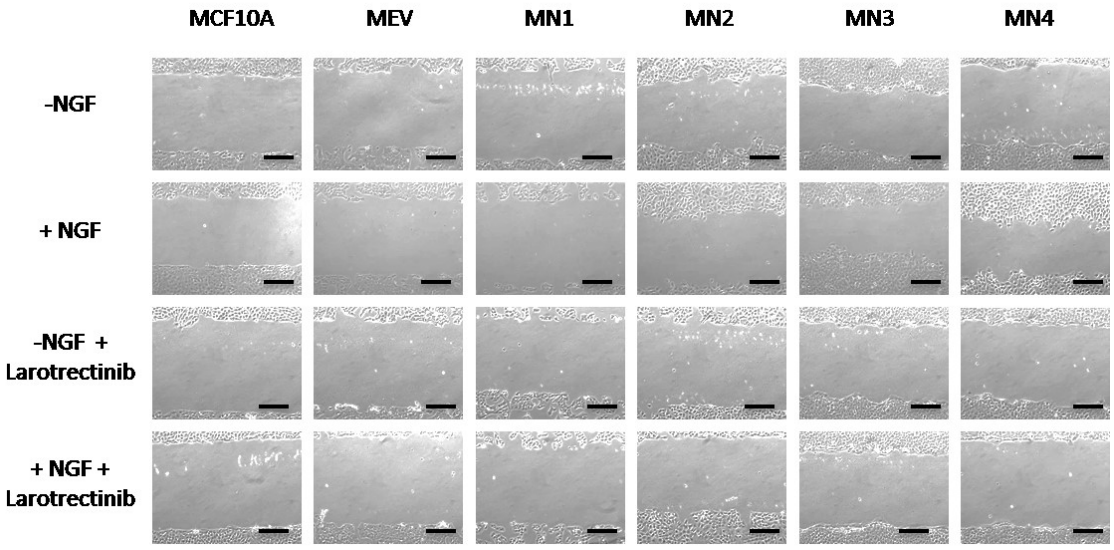

Figure 23: Representative images of MCF10A scratch assays. TrkA overexpressing clones MN1-4 supplemented with ligand NGF show uneven, wavy morphology in the advancing front at 16 hours (scale bar, 50 μm).

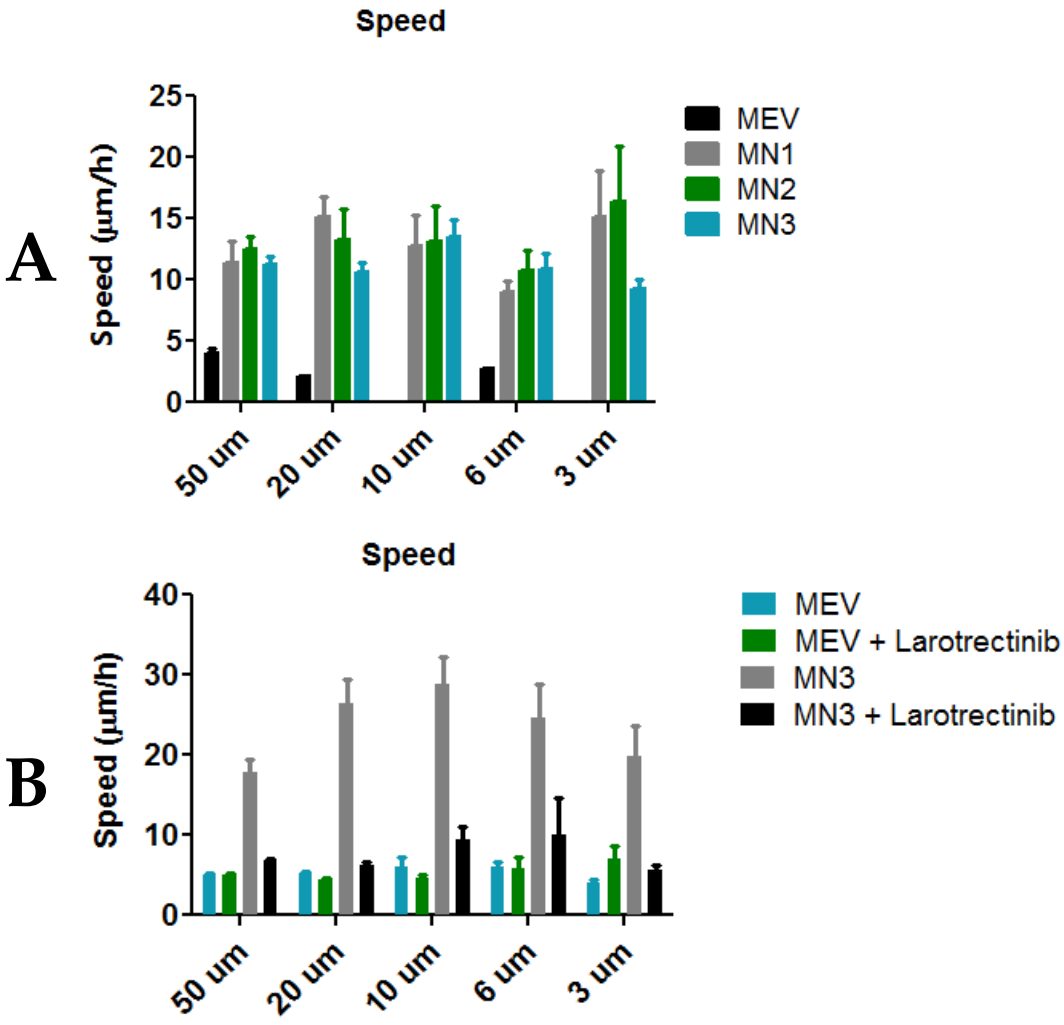

Figure 24: Microchannel migration assays were performed tracking individual cells across variously sized channels along a growth factor gradient. (A) TrkA overexpressing clone showed higher instantaneous speed (B) Larotrectinib reduced this effect.

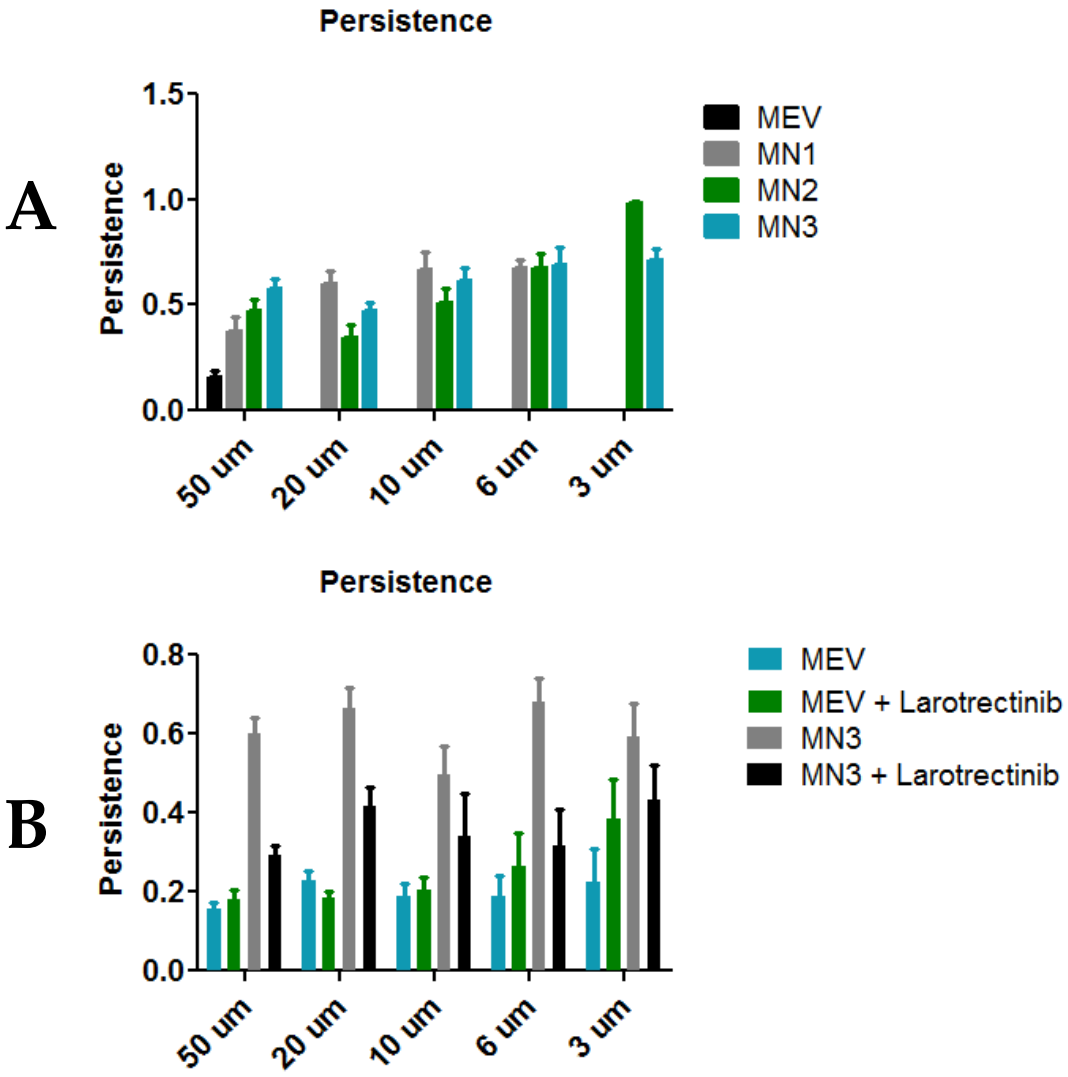

Figure 25: Microchannel migration assays were performed tracking individual cells across variously sized channels along a growth factor gradient. (A) TrkA overexpressing clone showed no significant difference in persistence (net cell displacement to total distance traveled) (B) Results were similar in the presence of larotrectinib.

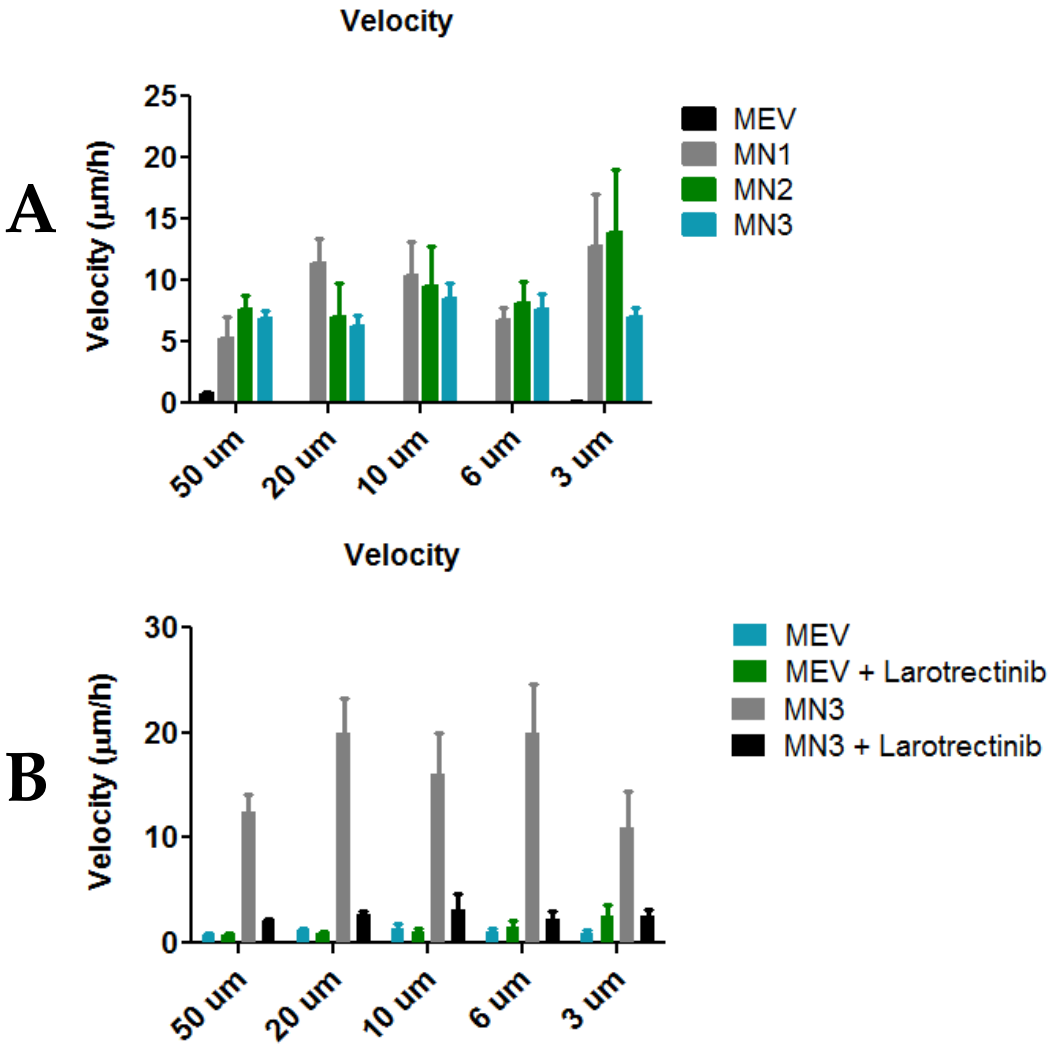

Figure 26: Microchannel migration assays were performed tracking individual cells across variously sized channels along a growth factor gradient. (A) TrkA overexpressing clone showed higher cellular velocity, calculated as the product of speed and persistence (B) Larotrectinib reduced this effect.

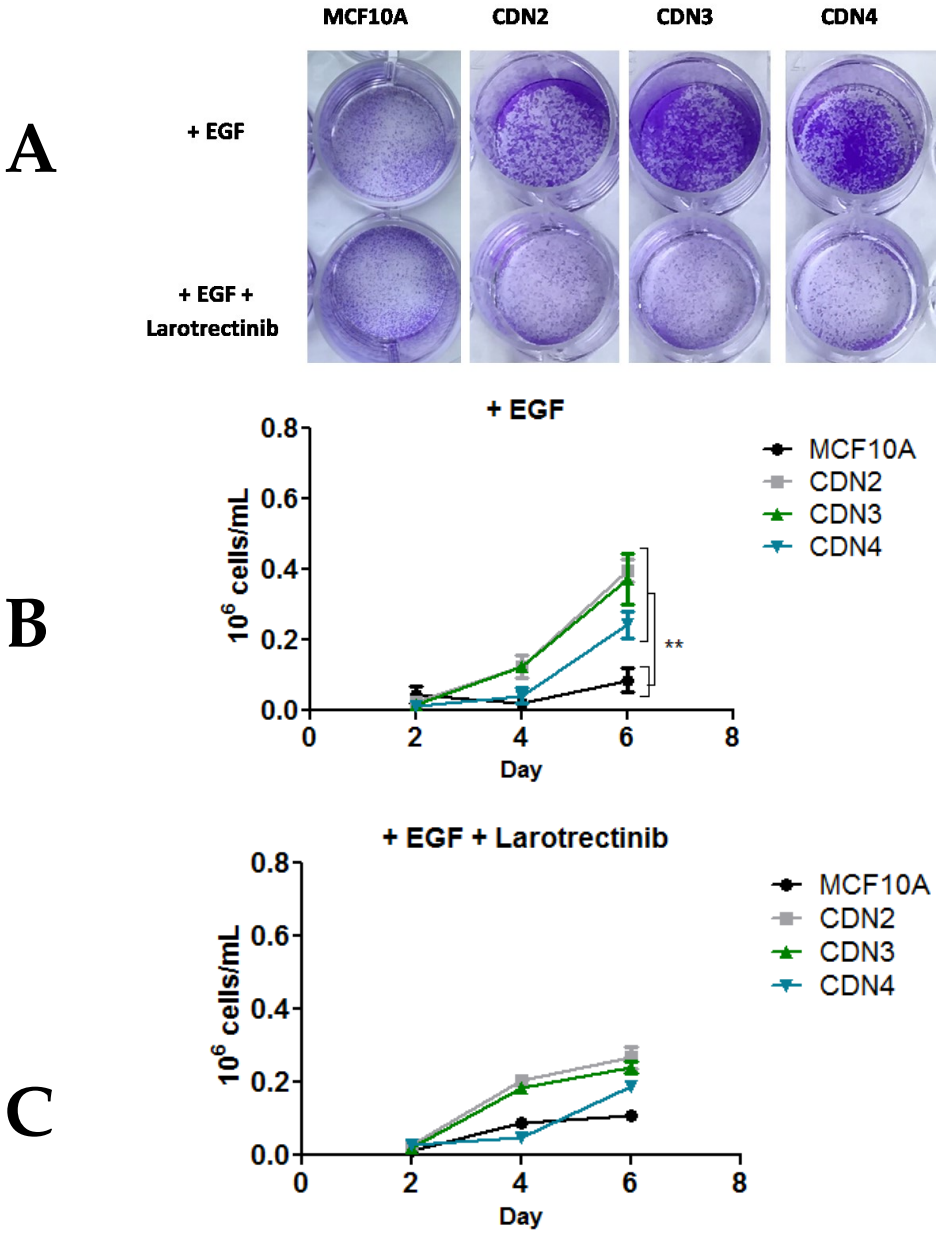

Figure 27: Modeling a *CD74-NTRK1* fusion expression in an MCF10A recapitulates growth advantage and larotrectinib sensitivity under growth-limiting media conditions as seen in TrkA overexpression model. *CD74-NTRK1* expressing isogenic clones (CDN2-4) show proliferative advantage over parental MCF10A in crystal violet (A) and cell counting (B,C), decreased by larotrectinib.

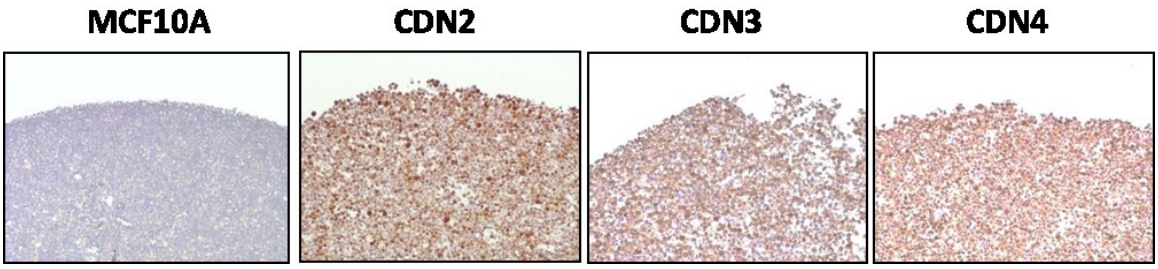

Figure 28: Confirmation of TrkA expression by immunohistochemistry; antibody binds region in fusion sequence. Cells were collected, pelleted, and pellets preserved in formalin before paraffin embedding, sectioning, and immunohistochemistry for TrkA motif.

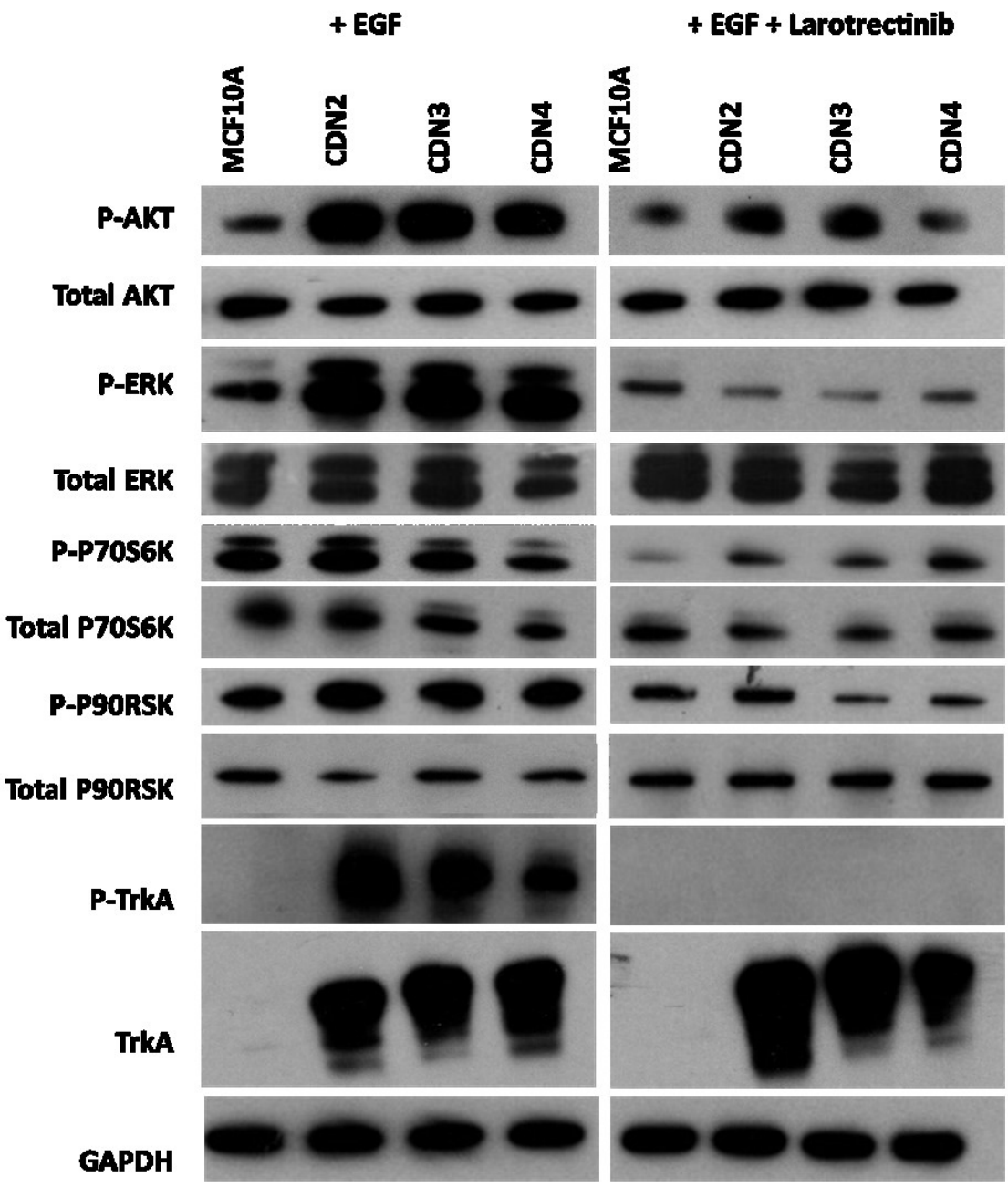

Figure 29: Modeling a *CD74-NTRK1* fusion expression in MCF10A recapitulates phosphorylation signaling amplification and larotrectinib sensitivity under growth-limiting media conditions as seen in TrkA overexpression model. Protein lysates were prepared from *CD74-NTRK1* fusion cell lines and parental MCF10A after 24 hours in arrest conditions with and without larotrectinib, subjected to western blot and probed for the specified antibodies. Phosphorylation of AKT, ERK, and P90RSK1 is increased in CDN clones, inhibited by larotrectinib.

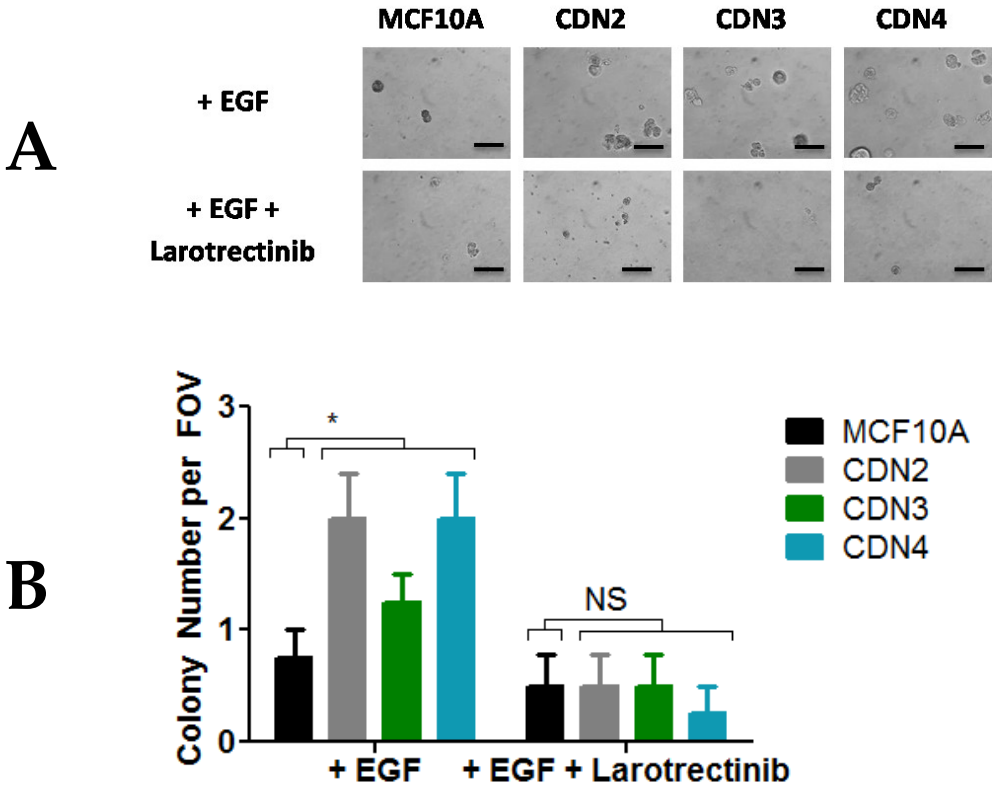

Figure 30: Modeling a *CD74-NTRK1* fusion expression in an MCF10A recapitulates morphology and anchorage independence in three-dimensional culture and larotrectinib sensitivity under growth-limiting media conditions as seen in TrkA overexpression model. Three-dimensional culture in Matrigel (A) and soft agar (B) gives slightly larger colonies, with larotrectinib reducing to parental size and number. FOV, field of view. Scale bar, 50 μm.

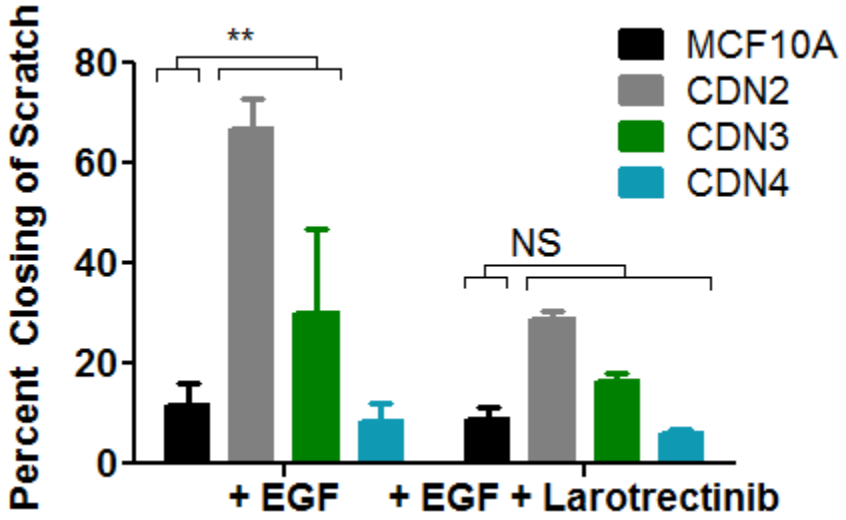

Figure 31: Modeling a *CD74-NTRK1* fusion expression in an MCF10A recapitulates increased wound healing, and larotrectinib sensitivity under growth-limiting media conditions as seen in TrkA overexpression model. Confluent monolayers were scratched and imaged at 0 and 16 hours, and percent closing of scratch calculated using MiToBo for ImageJ.

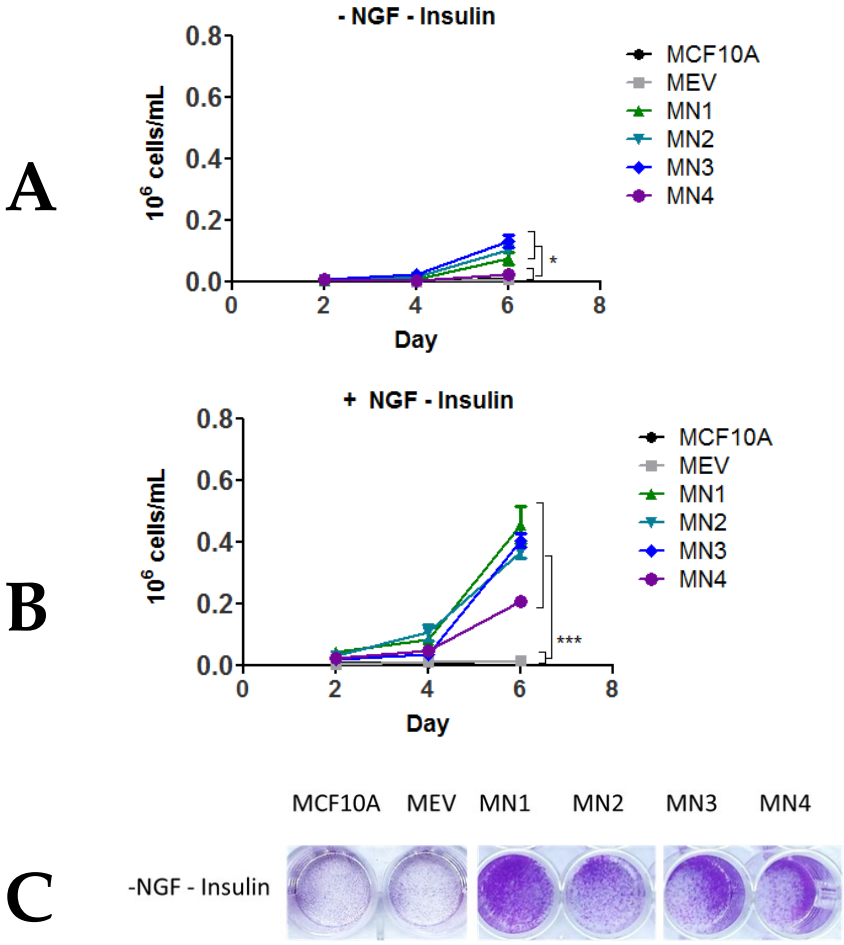

Figure 32: TrkA overexpression confers insulin independence. MCF10A parental cell line, MEV empty vector control, MN1-4 TrkA overexpression clones were plated at 30,000 cells/well and changed to insulin-free assay media with or without NGF at 100ng/mL after 24 hours. (A, B) Average proliferation as performed by cell counts on a Beckman Coulter cell counter at day 2, 4, 6 with and without NGF. (C) Crystal violet staining at 7 days.

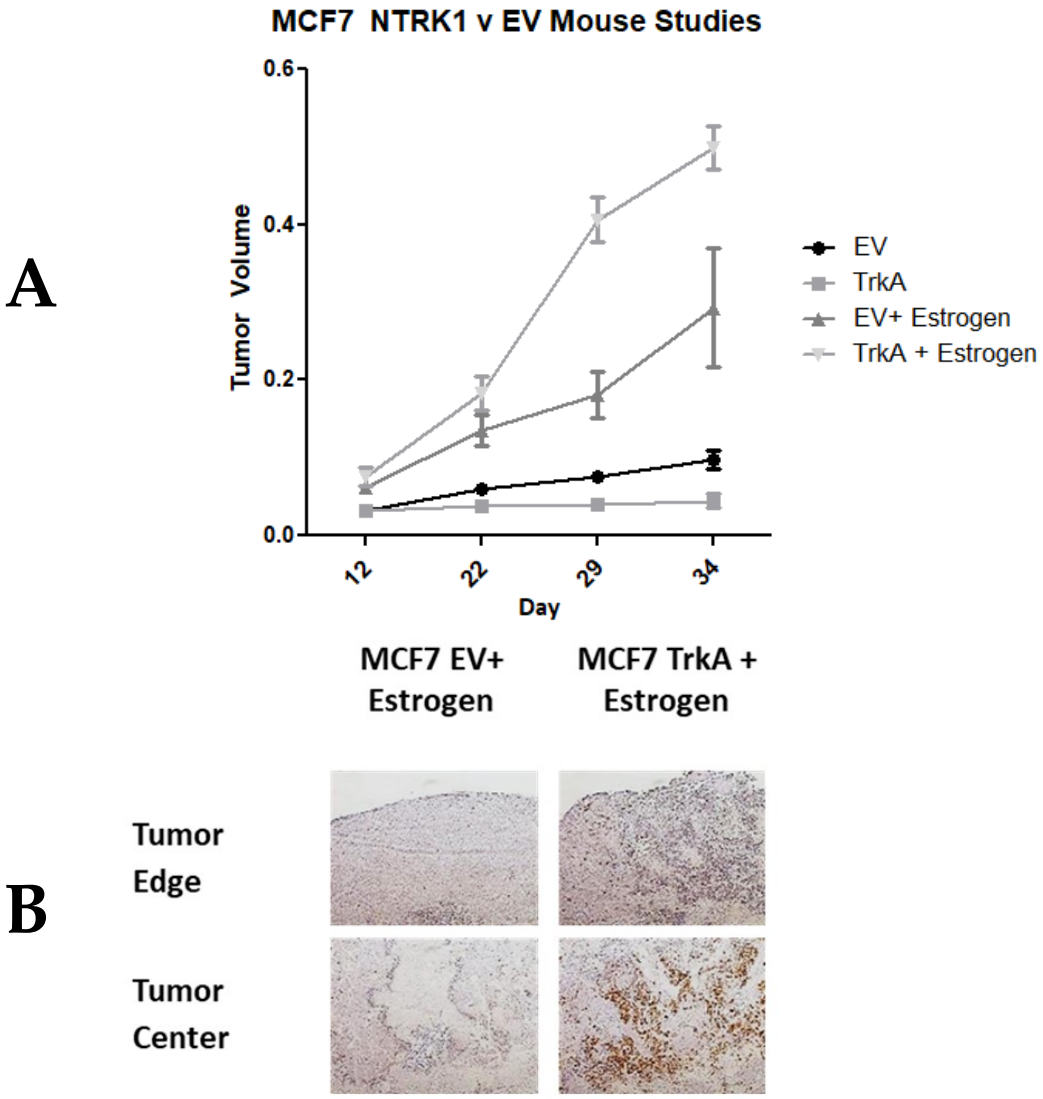

Figure 33: TrkA overexpressing isogenic clones of the tumorigenic breast line MCF7 were generated for *in vivo* work. NOD-SCID mice were injected subcutaneously with empty vector control or TrkA-overexpressing MCF7 cells. (A) TrkA overexpression gives a proliferative advantage but does not confer estrogen independence in MCF7. (B) TrkA expression in tumors confirmed by immunohistochemistry.

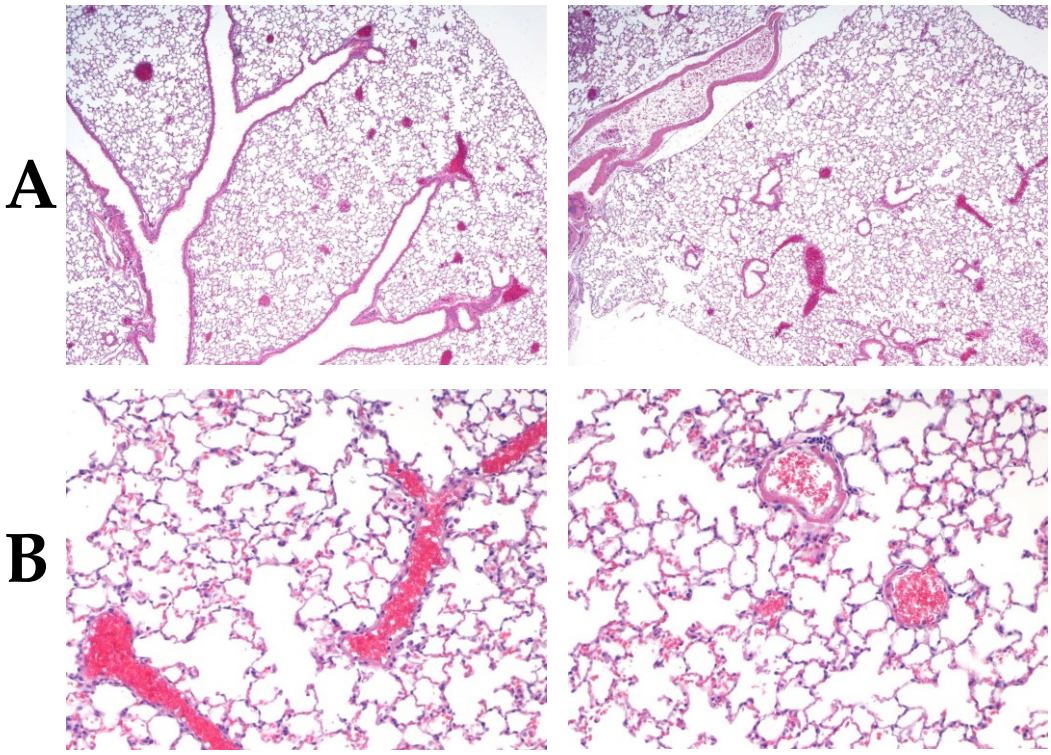

Figure 34: Representative images of lungs of mice after tail vein injection. MCF7 empty vector control does not form disseminated disease after tail vein injection. (A) Lung section, empty vector expressing MCF7, 4x. (B) Lung section, empty vector control expressing MCF7, 20x.

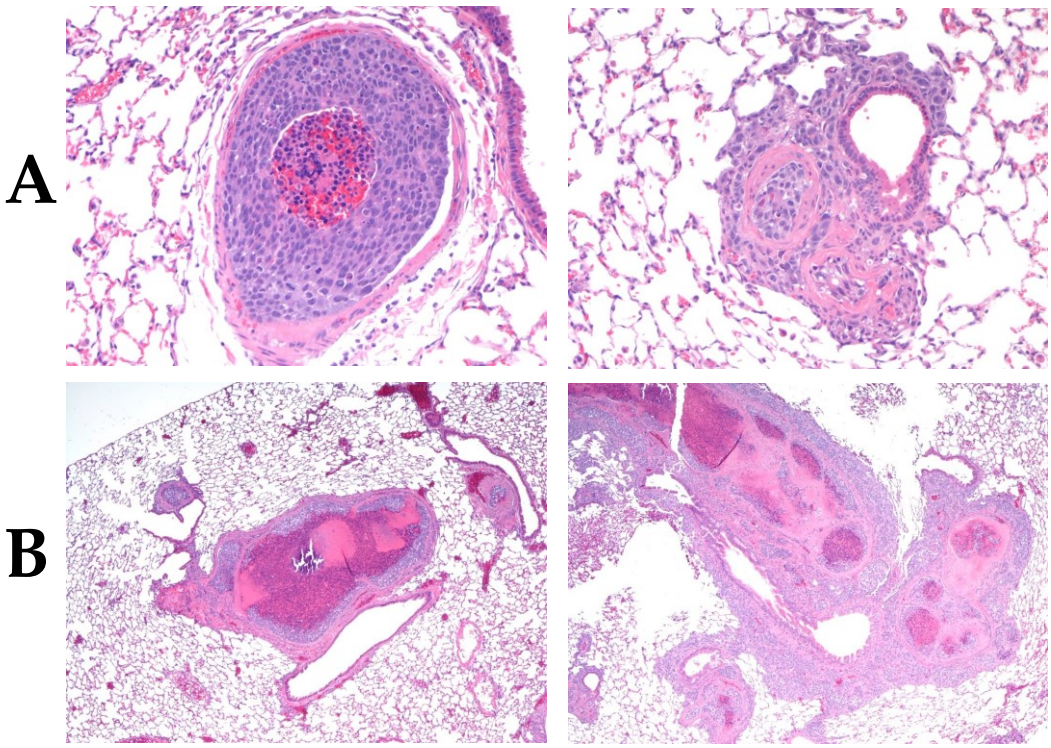

Figure 35: Representative images of lungs of mice after tail vein injection. TrkA overexpression in MCF7 confers the ability to form disseminated disease after tail vein injection. Small tumors adjacent to blood vessels as well as macroscopically visible tumors were formed in lung. (A) Lung section, TrkA-overexpressing MCF7, 4x. (B) Lung section, TrkA-overexpressing MCF7, 20x.

4 Discussion

As we delve deeper into mutational mapping of tumor formation and tumor progression, it is evident that personalizing medicine by targetable mutations will be more successful than by tissue of origin. Leveraging inhibitors designed for cancers of other origins to cross boundaries offers potential for intersecting extant therapies with new tumor types. Releasing the highly aggressive triple negative breast cancers from the limitations of cytotoxic chemotherapy, radiation and surgery is a key endeavor. The dramatic changes induced in this preclinical breast model with the overexpression seen in patients as well as its reversibility with larotrectinib give support to this intersecting approach in the model constructed for our studies. Here, our results

demonstrated the characteristics of TrkA amplification as a driver mutation in breast cancer across independent clones and multiple cell lines, and also suggest larotrectinib as a specific therapy in these models.

In our studies, we demonstrated that TrkA overexpression was transformative and targetable, causing amplification of cancer-associated phenotypes that was reversed under treatment with larotrectinib. TrkA overexpressors showed not only advantages in proliferation in both monolayer and three dimensional culture as well as signaling activation, but migratory alterations that could promote and assist metastasis. A putative autocrine TrkA-NGF loop has been established in the MCF7 cell line. Publications vary on the exact levels of neuronal growth factor present in breast and other tissues but agree on the presence of the ligand endogenously. Tumors expressing TrkA may have growth and migratory advantages, and the chemotactic migratory NGF pathway could promote metastasis and even contribute to the tropism of breast cancers to the NGF-high brain tissue. Notably, the enhanced tendency of the TrkA overexpressing cells to enter small channels in our migration assays, and not just the rate of migration, was reduced in kind by larotrectinib.

We recognize the limitations of our studies in modeling amplification of TrkA in breast cancer in that artificial transgene overexpression does not fully represent the range of amplification levels seen in patients, as well as the

potential positional effects of plasmid integration location. The latter we endeavored to minimize by studying multiple independent clones against both parental and empty vector controls in order to differentiate between clonal effects and the impact of the overexpression on phenotypes seen. The effectiveness of larotrectinib for breast cancer may indeed vary with the degree of amplification, which could perhaps be mitigated by setting a minimum threshold for treatment, similar to Herceptin in HER2 positive breast cancers. Additionally, the doses of larotrectinib required in order to inhibit these phenotypic changes were higher than anticipated. However, the doses required for the inhibition of the TrkA overexpression clones were matched to those required for our *in vitro* studies of the translocation clones, and given the significant responses to larotrectinib in translocations in ongoing clinical studies, we anticipate that this observation does not limit the potential clinical utility of larotrectinib for amplifications. Previous studies have also observed that high levels of various chemotherapeutic drugs are required to see effects in the non-tumorigenic MCF10A cell line (15).

Amplification of TrkA is broadly represented across numerous tumor types and multiple studies, suggesting a future for this inhibitor in a broad range of cancers showing this feature. Our study highlights migratory and metastatic

phenotypes as a key product of TrkA overexpression and validates the efficacy of larotrectinib in a TrkA overexpression model in breast cancer.

References

1. Khotskaya YB, Holla VR, Farago AF, Mills Shaw KR, Meric-Bernstam F, Hong DS. Targeting TRK family proteins in cancer. Pharmacol Ther. 2017;173:58-66. doi: 10.1016/j.pharmthera.2017.02.006. PubMed PMID: 28174090.

2. Badve S, Dabbs DJ, Schnitt SJ, Baehner FL, Decker T, Eusebi V, Fox SB, Ichihara S, Jacquemier J, Lakhani SR, Palacios J, Rakha EA, Richardson AL, Schmitt FC, Tan PH, Tse GM, Weigelt B, Ellis IO, Reis-Filho JS. Basal-like and triple-negative breast cancers: a critical review with an emphasis on the implications for pathologists and oncologists. Mod Pathol. 2011;24(2):157-67. doi: 10.1038/modpathol.2010.200. PubMed PMID: 21076464.

3. Hutchinson L. Breast cancer: TNBC: can we treat the untargetable? Nat Rev Clin Oncol. 2014;11(7):379. doi: 10.1038/nrclinonc.2014.88. PubMed PMID: 24840078.

4. Jamdade VS, Sethi N, Mundhe NA, Kumar P, Lahkar M, Sinha N. Therapeutic targets of triple-negative breast cancer: a review. Br J Pharmacol. 2015;172(17):4228-37. doi: 10.1111/bph.13211. PubMed PMID: 26040571; PMCID: PMC4556464.

5. Yam C, Mani SA, Moulder SL. Targeting the Molecular Subtypes of Triple Negative Breast Cancer: Understanding the Diversity to Progress the Field.

Oncologist. 2017;22(9):1086-93. doi: 10.1634/theoncologist.2017-0095. PubMed PMID: 28559413; PMCID: PMC5599192.

6. Andreopoulou E, Kelly CM, McDaid HM. Therapeutic Advances and New Directions for Triple-Negative Breast Cancer. Breast Care (Basel). 2017;12(1):21-8. doi: 10.1159/000455821. PubMed PMID: 28611537; PMCID: PMC5465752.

7. Hanahan D, Weinberg RA. Hallmarks of cancer: the next generation. Cell. 2011;144(5):646-74. doi: 10.1016/j.cell.2011.02.013. PubMed PMID: 21376230.

8. Doebele RC, Davis LE, Vaishnavi A, Le AT, Estrada-Bernal A, Keysar S, Jimeno A, Varella-Garcia M, Aisner DL, Li Y, Stephens PJ, Morosini D, Tuch BB, Fernandes M, Nanda N, Low JA. An Oncogenic NTRK Fusion in a Patient with Soft-Tissue Sarcoma with Response to the Tropomyosin-Related Kinase Inhibitor LOXO-101. Cancer Discov. 2015;5(10):1049-57. doi: 10.1158/2159-8290.CD-15-0443. PubMed PMID: 26216294; PMCID: PMC4635026.

9. Tian Q, Du P, Li S, Bai Z, Yang Y, Zeng J. Effect of antitumor treatments on triple-negative breast cancer patients: A PRISMA-compliant network meta-analysis of randomized controlled trials. Medicine (Baltimore). 2017;96(45):e8389. doi: 10.1097/MD.0000000000008389. PubMed PMID: 29137021; PMCID: PMC5690714.

10. Drilon A, Laetsch TW, Kummar S, DuBois SG, Lassen UN, Demetri GD, Nathenson M, Doebele RC, Farago AF, Pappo AS, Turpin B, Dowlati A, Brose MS, Mascarenhas L, Federman N, Berlin J, El-Deiry WS, Baik C, Deeken J, Boni V, Nagasubramanian R, Taylor M, Rudzinski ER, Meric-Bernstam F, Sohal DPS, Ma PC, Raez LE, Hechtman JF, Benayed R, Ladanyi M, Tuch BB, Ebata K, Cruickshank S, Ku NC, Cox MC, Hawkins DS, Hong DS, Hyman DM. Efficacy of Larotrectinib in TRK Fusion-Positive Cancers in Adults and Children. N Engl J Med. 2018;378(8):731-9. doi: 10.1056/NEJMoa1714448. PubMed PMID: 29466156.

11. Tan PS, Bilger M, de Lima Lopes G, Acharyya S, Haaland B. Meta-analysis of first-line therapies with maintenance regimens for advanced non-small-cell lung cancer (NSCLC) in molecularly and clinically selected populations. Cancer Med. 2017;6(8):1847-60. doi: 10.1002/cam4.1101. PubMed PMID: 28675660; PMCID: PMC5548880.

12. Dolle L, Adriaenssens E, El Yazidi-Belkoura I, Le Bourhis X, Nurcombe V, Hondermarck H. Nerve growth factor receptors and signaling in breast cancer. Curr Cancer Drug Targets. 2004;4(6):463-70. PubMed PMID: 15379632.

13. Descamps S, Toillon RA, Adriaenssens E, Pawlowski V, Cool SM, Nurcombe V, Le Bourhis X, Boilly B, Peyrat JP, Hondermarck H. Nerve growth factor stimulates proliferation and survival of human breast cancer cells through

two distinct signaling pathways. J Biol Chem. 2001;276(21):17864-70. doi: 10.1074/jbc.M010499200. PubMed PMID: 11359788.

14. Dolle L, El Yazidi-Belkoura I, Adriaenssens E, Nurcombe V, Hondermarck H. Nerve growth factor overexpression and autocrine loop in breast cancer cells. Oncogene. 2003;22(36):5592-601. doi: 10.1038/sj.onc.1206805. PubMed PMID: 12944907.

15. Drilon A, Siena S, Ou SI, Patel M, Ahn MJ, Lee J, Bauer TM, Farago AF, Wheler JJ, Liu SV, Doebele R, Giannetta L, Cerea G, Marrapese G, Schirru M, Amatu A, Bencardino K, Palmeri L, Sartore-Bianchi A, Vanzulli A, Cresta S, Damian S, Duca M, Ardini E, Li G, Christiansen J, Kowalski K, Johnson AD, Patel R, Luo D, Chow-Maneval E, Hornby Z, Multani PS, Shaw AT, De Braud FG. Safety and Antitumor Activity of the Multitargeted Pan-TRK, ROS1, and ALK Inhibitor Entrectinib: Combined Results from Two Phase I Trials (ALKA-372-001 and STARTRK-1). Cancer Discov. 2017;7(4):400-9. doi: 10.1158/2159-8290.CD-16-1237. PubMed PMID: 28183697; PMCID: PMC5380583.

16. Vaishnavi A, Capelletti M, Le AT, Kako S, Butaney M, Ercan D, Mahale S, Davies KD, Aisner DL, Pilling AB, Berge EM, Kim J, Sasaki H, Park S, Kryukov G, Garraway LA, Hammerman PS, Haas J, Andrews SW, Lipson D, Stephens PJ, Miller VA, Varella-Garcia M, Janne PA, Doebele RC. Oncogenic and drug-

sensitive NTRK1 rearrangements in lung cancer. Nat Med. 2013;19(11):1469-72. doi: 10.1038/nm.3352. PubMed PMID: 24162815; PMCID: PMC3823836.

17. Zabransky DJ, Yankaskas CL, Cochran RL, Wong HY, Croessmann S, Chu D, Kavuri SM, Red Brewer M, Rosen DM, Dalton WB, Cimino-Mathews A, Cravero K, Button B, Kyker-Snowman K, Cidado J, Erlanger B, Parsons HA, Manto KM, Bose R, Lauring J, Arteaga CL, Konstantopoulos K, Park BH. HER2 missense mutations have distinct effects on oncogenic signaling and migration. Proc Natl Acad Sci U S A. 2015;112(45):E6205-14. doi: 10.1073/pnas.1516853112. PubMed PMID: 26508629; PMCID: PMC4653184.

18. Wong HY, Wang GM, Croessmann S, Zabransky DJ, Chu D, Garay JP, Cidado J, Cochran RL, Beaver JA, Aggarwal A, Liu ML, Argani P, Meeker A, Hurley PJ, Lauring J, Park BH. TMSB4Y is a candidate tumor suppressor on the Y chromosome and is deleted in male breast cancer. Oncotarget. 2015;6(42):44927-40. doi: 10.18632/oncotarget.6743. PubMed PMID: 26702755; PMCID: PMC4792601.

19. Wang GM, Wong HY, Konishi H, Blair BG, Abukhdeir AM, Gustin JP, Rosen DM, Denmeade SR, Rasheed Z, Matsui W, Garay JP, Mohseni M, Higgins MJ, Cidado J, Jelovac D, Croessmann S, Cochran RL, Karnan S, Konishi Y, Ota A, Hosokawa Y, Argani P, Lauring J, Park BH. Single copies of mutant KRAS and mutant PIK3CA cooperate in immortalized human epithelial cells to induce

tumor formation. Cancer Res. 2013;73(11):3248-61. doi: 10.1158/0008-5472.CAN-12-1578. PubMed PMID: 23580570; PMCID: PMC3674106.

20. Choong LY, Lim S, Chong PK, Wong CY, Shah N, Lim YP. Proteome-wide profiling of the MCF10AT breast cancer progression model. PLoS One. 2010;5(6):e11030. doi: 10.1371/journal.pone.0011030. PubMed PMID: 20543960; PMCID: PMC2882958.

21. Narayan S, Jaiswal AS, Law BK, Kamal MA, Sharma AK, Hromas RA. Interaction between APC and Fen1 during breast carcinogenesis. DNA Repair (Amst). 2016;41:54-62. doi: 10.1016/j.dnarep.2016.04.003. PubMed PMID: 27088617; PMCID: PMC4851606.

22. Abdel-Fatah TM, Russell R, Albarakati N, Maloney DJ, Dorjsuren D, Rueda OM, Moseley P, Mohan V, Sun H, Abbotts R, Mukherjee A, Agarwal D, Illuzzi JL, Jadhav A, Simeonov A, Ball G, Chan S, Caldas C, Ellis IO, Wilson DM, 3rd, Madhusudan S. Genomic and protein expression analysis reveals flap endonuclease 1 (FEN1) as a key biomarker in breast and ovarian cancer. Mol Oncol. 2014;8(7):1326-38. doi: 10.1016/j.molonc.2014.04.009. PubMed PMID: 24880630; PMCID: PMC4690463.

23. Hilborn E, Stal O, Alexeyenko A, Jansson A. The regulation of hydroxysteroid 17beta-dehydrogenase type 1 and 2 gene expression in breast cancer cell lines by estradiol, dihydrotestosterone, microRNAs, and genes related

to breast cancer. Oncotarget. 2017;8(37):62183-94. doi: 10.18632/oncotarget.19136. PubMed PMID: 28977936; PMCID: PMC5617496.

24. Hilborn E, Stal O, Jansson A. Estrogen and androgen-converting enzymes 17beta-hydroxysteroid dehydrogenase and their involvement in cancer: with a special focus on 17beta-hydroxysteroid dehydrogenase type 1, 2, and breast cancer. Oncotarget. 2017;8(18):30552-62. doi: 10.18632/oncotarget.15547. PubMed PMID: 28430630; PMCID: PMC5444764.

25. Liu S, Lee JS, Jie C, Park MH, Iwakura Y, Patel Y, Soni M, Reisman D, Chen H. HER2 overexpression triggers an IL-1alpha pro-inflammatory circuit to drive tumorigenesis and promote chemotherapy resistance. Cancer Res. 2018. doi: 10.1158/0008-5472.CAN-17-2761. PubMed PMID: 29382706.

26. Han SJ, Begum K, Foulds CE, Hamilton RA, Bailey S, Malovannaya A, Chan D, Qin J, O'Malley BW. The Dual Estrogen Receptor alpha Inhibitory Effects of the Tissue-Selective Estrogen Complex for Endometrial and Breast Safety. Mol Pharmacol. 2016;89(1):14-26. doi: 10.1124/mol.115.100925. PubMed PMID: 26487511; PMCID: PMC4702103.

27. Hebbar N, Burikhanov R, Shukla N, Qiu S, Zhao Y, Elenitoba-Johnson KSJ, Rangnekar VM. A Naturally Generated Decoy of the Prostate Apoptosis Response-4 Protein Overcomes Therapy Resistance in Tumors. Cancer Res.

2017;77(15):4039-50. doi: 10.1158/0008-5472.CAN-16-1970. PubMed PMID: 28625975; PMCID: PMC5540761.

28. Boudreau A, Tanner K, Wang D, Geyer FC, Reis-Filho JS, Bissell MJ. 14-3-3sigma stabilizes a complex of soluble actin and intermediate filament to enable breast tumor invasion. Proc Natl Acad Sci U S A. 2013;110(41):E3937-44. doi: 10.1073/pnas.1315022110. PubMed PMID: 24067649; PMCID: PMC3799319.

29. Pu SY, Yu Q, Wu H, Jiang JJ, Chen XQ, He YH, Kong QP. ERCC6L, a DNA helicase, is involved in cell proliferation and associated with survival and progress in breast and kidney cancers. Oncotarget. 2017;8(26):42116-24. doi: 10.18632/oncotarget.14998. PubMed PMID: 28178669; PMCID: PMC5522053.

30. Husa AM, Magic Z, Larsson M, Fornander T, Perez-Tenorio G. EPH/ephrin profile and EPHB2 expression predicts patient survival in breast cancer. Oncotarget. 2016;7(16):21362-80. doi: 10.18632/oncotarget.7246. PubMed PMID: 26870995; PMCID: PMC5008291.

31. Lam S, Wiercinska E, Teunisse AF, Lodder K, ten Dijke P, Jochemsen AG. Wild-type p53 inhibits pro-invasive properties of TGF-beta3 in breast cancer, in part through regulation of EPHB2, a new TGF-beta target gene. Breast Cancer Res Treat. 2014;148(1):7-18. doi: 10.1007/s10549-014-3147-8. PubMed PMID: 25257729.

32. Chukkapalli S, Amessou M, Dilly AK, Dekhil H, Zhao J, Liu Q, Bejna A, Thomas RD, Bandyopadhyay S, Bismar TA, Neill D, Azoulay L, Batist G, Kandouz M. Role of the EphB2 receptor in autophagy, apoptosis and invasion in human breast cancer cells. Exp Cell Res. 2014;320(2):233-46. doi: 10.1016/j.yexcr.2013.10.022. PubMed PMID: 24211352.

33. Sekiya R, Maeda M, Yuan H, Asano E, Hyodo T, Hasegawa H, Ito S, Shibata K, Hamaguchi M, Kikkawa F, Kajiyama H, Senga T. PLAGL2 regulates actin cytoskeletal architecture and cell migration. Carcinogenesis. 2014;35(9):1993-2001. doi: 10.1093/carcin/bgu081. PubMed PMID: 24675530.

34. Riku M, Inaguma S, Ito H, Tsunoda T, Ikeda H, Kasai K. Down-regulation of the zinc-finger homeobox protein TSHZ2 releases GLI1 from the nuclear repressor complex to restore its transcriptional activity during mammary tumorigenesis. Oncotarget. 2016;7(5):5690-701. doi: 10.18632/oncotarget.6788. PubMed PMID: 26744317; PMCID: PMC4868714.

35. Tynan SH, Lundeen SG, Allan GF. Cell type-specific bidirectional regulation of the glucocorticoid-induced leucine zipper (GILZ) gene by estrogen. J Steroid Biochem Mol Biol. 2004;91(4-5):225-39. doi: 10.1016/j.jsbmb.2004.05.002. PubMed PMID: 15336700.

Curriculum Vitae

Kelly Kyker-Snowman March 2018
1650 Orleans St., CRBI, Room 116
Baltimore, MD 21287
Phone: 443-287-4480
Fax: 410-614-4073
Email: kkykers1@jhmi.edu

Education and Training

Ph.D. May 2018	The Johns Hopkins School of Medicine Cellular and Molecular Medicine, mentor Ben Park
M.S. May 2010	University of Rochester Biomedical Engineering, Cell and Tissue Engineering
B.S. May 2009	University of Rochester Biomedical Engineering, Cell and Tissue Engineering, Cum Laude High Distinction

Professional Experience

2/2011 – 8/2013	Lab Technician III, Nephrology, University of Rochester School of Medicine, Krieger Lab
1/2009-5/2010	Research Intern, University of Rochester School of Medicine and Dentistry, Brown Lab
6/2008-8/2008	Research Intern, Pioneer Valley Life Science Institute, Schneyer Lab

Research Support

9/2014-8/2015	NIH National Cancer Institute Cancer Research Training Grant 5T32GM008752-15
9/2013-8/2014	NIH National Cancer Institute Cancer Research Training Grant 5T32GM008752-14

Awards, Honors

2018	Urban Health Institute Student-Community Small Grant Award
2005-2009	Dean's List

Peer Reviewed Original Science Research

1. **Kyker-Snowman K**, Avigdor B, Nasim M, Cimino-Mathews A, Wheelan SJ, Argani P, Park BH. A primary breast cancer with distinct foci of estrogen receptor alpha positive and negative cells derived from the same clonal origin as revealed by whole exome sequencing. Breast Cancer Research and Treatment. In press, 2018.
2. Avigdor B, Beierl K, Gocke CD, Zabransky D, Cravero K, **Kyker-Snowman K**, Button B, Chu D, Croessmann S, Cochran RL, Connolly R, Park BH*, Wheelan SJ*, Cimino-Mathews A*. Whole exome sequencing of metaplastic breast carcinoma indicates monoclonality with associated ductal carcinoma component. *Clin Cancer Res.* August 2017. *Co-corresponding author.
3. Croessmann S, Wong HY, Zabransky DJ, Chu D, Rosen DM, Cidado J, Cochran RL, Dalton WB, Erlanger B, Cravero K, Button B, **Kyker-Snowman K**, Hurley PJ, Lauring J, Park BH**.** PIK3CA mutations and TP53 alterations cooperate to increase cancerous phenotypes and tumor heterogeneity. *Breast Cancer Res Treat,* Apr;162(3):451-464, 2017.
4. Lee J, Axilbund J, Dalton BD, Laheru D, Watkins S, Chu D, Cravero K, Button B, **Kyker-Snowman K**, Waters I, Gocke C, Lauring J and Park BH. A polycythemia vera JAK2 mutation masquerading as a germline cancer mutation in a patient with duodenal cancer, *The Journal of the National Comprehensive Cancer Network*, Dec;14(12):1495-1498, 2016.
5. Krieger NS, Yao Z, **Kyker-Snowman** K, Kim MH, Boyce BF, Bushinsky DA. Increased bone density in mice lacking the proton receptor OGR1. *Kidney International*. 2016 Mar;89(3):565-7. Epub 2016 Jan 6.
6. Zabransky DJ, Yankaskas CL, Cochran RL, Wong HY, Croessmann S, Chu D, Kavuri SM, Brewer MR, Rosen DM, Dalton WB, Cimino-Mathews A, Cravero K, Button B, **Kyker-Snowman K**, Cidado J, Erlanger B, Parsons H, Manto KM, Bose R, Lauring J, Arteaga CL, Konstantopoulos K, Park BH. HER2 missense mutations have distinct effects on oncogenic signaling and migration. *Proc Natl Acad Sci U S A.* Nov 10;112(45), 2015.
7. Chu D, Paoletti C, Gersch C, VanDenBerg DA, Zabransky DJ, Cochran RL, Wong HY, Toro PV, Cidado J, Croessmann S, Erlanger B, Cravero K, **Kyker-Snowman K**, Button B, Parsons H, Dalton BD, Gillani R, Medford A, Aung K, Tokudome N, Chinnaiyan A, Schott A, Robertson D, Jacks KS, Lauring J, Hurley P, Hayes DF, Rae JM and Park BH. ESR1 mutations in circulating plasma tumor DNA from metastatic breast cancer patients. *Clinical Cancer Research*, Feb 15;22(4):993-9, 2016.

8. Croessmann S, Wong HY, Zabransky DJ, Chu D, Mendonca J, Sharma A, Mohseni M, Rosen DM, Scharpf R, Cidado J, Cochran RL, Parsons H, Dalton WB, Erlanger B, Button B, Cravero K, **Kyker-Snowman K**, Beaver JA, Kachhap S, Hurley PJ, Lauring J, Park BH. NDRG1 links p53 with proliferation mediated centrosome homeostasis and genome stability. *Proc Natl Acad Sci U S A.* Sep 15;112(37):11583-8, 2015.
9. Ng AH, Frick KK, Krieger NS, Asplin JR, Cohen-McFarlane M, Culbertson CD, **Kyker-Snowman K**, Grynpas MD, Bushinsky DA. $1,25(OH)_2D_3$ induces a mineralization defect and loss of bone mineral density in genetic hypercalciuric stone-forming rats. *Calcified Tissue International*. 2014 May;94(5):531-43. Epub 2014 Jan 31.
10. Krieger NS, Culbertson CD, **Kyker-Snowman K**, Bushinsky DA. Metabolic acidosis increases fibroblast growth factor 23 in neonatal mouse bone. *American Journal of Physiology - Renal Physiology*. 2012 Aug 1;303(3):F431-6. Epub 2012 May 30.

Book Chapters

1. **Kyker-Snowman K**, Park BH. "Circulating Free Tumor DNA (ctDNA): The Real-Time Liquid Biopsy" Liquid Biopsies in Solid Tumors, pp 105-118, Springer, 2017.

Posters and Presentations

2017 **Kyker-Snowman K**. *NTRK1 in Breast Cancer*, Cellular and Molecular Medicine Retreat, Johns Hopkins University School of Medicine, Baltimore, MD
2016 **Kyker-Snowman K**. *Oncogenic Properties and Targeting of NTRK1 in Breast Cancer,* Cellular and Molecular Medicine Retreat, Johns Hopkins University School of Medicine, Baltimore, MD
2015 **Kyker-Snowman K**. *NTRK1 in Breast and Ovarian Cancers* Cellular and Molecular Medicine Retreat, Johns Hopkins University School of Medicine, Baltimore, MD
2012 Krieger NS, Yao Z, **Kyker-Snowman K**, Boyce B, Bushinsky DA. *Increased bone density in mice lacking the proton receptor OGR1*. American Society for Bone and Mineral Research Annual Meeting, October 2012.
2012 Krieger NS, Culbertson C, **Kyker-Snowman K**, Bushinsky DA. *Metabolic acidosis increases fibroblast growth factor 23 in neonatal mouse bone.* American Society for Bone and Mineral Research Annual Meeting, October 2012.
2012 Krieger NS, Culbertson C, **Kyker-Snowman K**, Bushinsky DA. *Stimulation of RANKL and bone resorption by metabolic acidosis requires Gbg*

signaling. American Society for Bone and Mineral Research Annual Meeting, Septmeber 2011.
2011 Frick KK, Asplin J, Granja I, Krieger NS, Culbertson C, **Kyker-Snowman K**, Bushinsky DA. *Inhibition of Bone Resorption Suppresses 1,25(OH)2D3-Induced Hypercalciuria in Genetic Hypercalciuric Stone-Forming Rats*. 45th Annual Meeting, American Society for Nephrology, San Diego, CA, November 2011.

Inventions

05/18/15	C13626 Overexpression of ntrk1 cDNA in the Nontumorgenic Breast Epithelial Cell Line MCF-10A, **Kyker-Snowman, Kelly** and Park BH

Classroom Instruction

2013-2016	MCAT Instructor, Content Developer, Kaplan
1/2010-5/2010	Teaching Assistant, Biomedical Engineering Senior Design, University of Rochester Biomedical Engineering Department
9/2008-5/2010	Laboratory Teaching Assistant, University of Rochester Chemistry Department
9/2009-12/2009	Workshop Leader, Cell Biology, University of Rochester Biology Department

Professional Societies

2005 – 2009	Alpha Eta Mu Beta Biomedical Engineering Honor Society
2005 – present	Society of Women Engineers
2005 – present	Biomedical Engineering Society
2015 – present	American Association for the Advancement of Science

Community Service

2013-2018	Baltimore Dance Crews Project, Data Specialist, Impact Coordinator and Mentor